

**ASSESSMENT OF PROBABILITY OF  
LOCALIZED CORROSION OF ALLOY 22 WASTE  
PACKAGE MATERIAL**

*Prepared for*

**U.S. Nuclear Regulatory Commission  
Contract NRC-02-07-006**

*Prepared by*

**O. Pensado  
R.T. Pabalan**

**Center for Nuclear Waste Regulatory Analyses  
San Antonio, Texas**

**September 2011**

## ABSTRACT

A key attribute of the U.S. Department of Energy (DOE) safety strategy for the high-level nuclear waste repository it proposed to construct at Yucca Mountain, Nevada, included long-lived waste packages comprising an outer container of a highly corrosion-resistant nickel–chromium–molybdenum alloy (Alloy 22) over an inner container made of Type 316 nuclear grade stainless steel. In the absence of mechanical disruption, DOE expected aqueous corrosion to be the primary degradation process limiting the life of the waste packages. The mode and rate of corrosion of the waste package materials were expected to depend on the chemistry of water contacting them and on temperature. Coupled thermal-hydrological-chemical processes would significantly alter the chemistry of groundwater that seeps into the repository drift and contacts the waste packages and drip shields. Radioactive decay can cause waste packages and drip shields to experience transient temperatures above the boiling point of pure water for several hundreds to few thousands of years. During this transient elevated temperature period, seepage water evaporation could lead to the formation of corrosive brines on waste package surfaces and promote localized corrosion of the waste package material.

This report documents an analysis of the likelihood of environmental conditions established by seepage water evaporation capable of supporting initiation and propagation of localized corrosion of the Alloy 22 waste package material. The analysis accounts for the variability in solution composition and temperature of the Alloy 22 material and is based on the concept of corrosion and repassivation potentials and their dependence on the chemistry of brines that may evolve from seepage water evaporation.

The results indicate that Alloy 22 localized corrosion is likely (probability  $>0.001$ ) only at temperature ( $T$ )  $>80\text{ }^{\circ}\text{C}$  [ $>176\text{ }^{\circ}\text{F}$ ]. At  $T \leq 80\text{ }^{\circ}\text{C}$  [ $\leq 176\text{ }^{\circ}\text{F}$ ], the solutions contacting the waste package material will have a sufficiently high pH such that localized corrosion (i.e.,  $E_{\text{corr}} > E_{\text{rcrev}}$ ) is unlikely (probability  $<0.001$ ). The analysis also indicates that when  $T < 50\text{ }^{\circ}\text{C}$  [ $<122\text{ }^{\circ}\text{F}$ ] and a marginal amount of nitrate is present in solution, the solution pH is unlikely to be low enough to cause localized corrosion.

The DOE equations imply that increasing chloride concentrations could have a beneficial effect on localized corrosion. It is hypothesized that increasing concentrations of chloride displace oxygen and other oxidants in the solution causing the corrosion potential to decrease. On the other hand, increasing chloride concentration causes the repassivation potential to decrease. The net effect of these competing trends is the nonintuitive result that localized corrosion is less likely in solutions of increasing chloride concentration. This nonintuitive trend was used to rationalize DOE results that showed varying probability for localized corrosion as a function of deep percolation rates (DOE divided the repository into five percolation bins). The probability of localized corrosion is slightly higher in the midrange of the considered percolation bins. For the low percolation rate region, the temperature tends to be higher and the system drier, causing chloride concentrations to be higher and localized corrosion to be less likely. For the high percolation rate region, the temperature is lower, the relative humidity higher, and the range of pH tends to be higher, which makes localized corrosion less likely. The analysis indicates that in the midrange of the percolation rates—where the temperature and relative humidity are comparatively high to cause solutions with low pH and low chloride concentration to form—localized corrosion has a slightly higher chance of occurrence, in agreement with the results of DOE calculations. The prediction of localized corrosion in solutions of low chloride concentration and low temperature, however, is most likely an artifact of the mathematical curve fitting because localized corrosion of Alloy 22 has never been detected in this type of environment.

## CONTENTS

Section	Page
ABSTRACT	ii
FIGURES	v
TABLES	vii
ACKNOWLEDGMENTS .....	viii
1 INTRODUCTION .....	1-1
2 CHEMISTRY OF SOLUTIONS CONTACTING WASTE PACKAGES AND DRIP SHIELDS .....	2-1
3 ASSESSMENT OF DOE LOCALIZED CORROSION MODEL.....	3-1
4 SUMMARY AND CONCLUSIONS.....	4-1
5 REFERENCES .....	5-1

## FIGURES

### Figure Page

2-1	Composition of Yucca Mountain Unsaturated Zone Waters .....	2-2
2-2	Calculated pHs of Brines Resulting From Evaporation of Yucca Mountain Unsaturated Zone Waters at 25, 50, 70, 90, and 100 °C [77, 122, 158, 194, and 230 °F] and Total Pressure Corresponding to $RH_{median}$ .....	2-5
2-3	Calculated $Na^+$ Concentrations of Brines Resulting From Evaporation of Yucca Mountain Unsaturated Zone Waters at 25, 50, 70, 90, and 100 °C [77, 122, 158, 194, and 230 °F] and Total Pressure Corresponding to $RH_{median}$ .....	2-6
2-4	Calculated $Mg^{2+}$ Concentration of Brines Resulting From Evaporation of Yucca Mountain Unsaturated Zone Waters at 25, 50, 70, 90, and 100 °C [77, 122, 158, 194, and 230 °F] and Total Pressure Corresponding to $RH_{median}$ .....	2-7
2-5	Calculated $Ca^{2+}$ Concentrations of Brines Resulting From Evaporation of Yucca Mountain Unsaturated Zone Waters at 25, 50, 70, 90, and 100 °C [77, 122, 158, 194, and 230 °F] and Total Pressure Corresponding to $RH_{median}$ .....	2-8
2-6	Calculated $Cl^-$ Concentrations of Brines Resulting From Evaporation of Yucca Mountain Unsaturated Zone Waters at 25, 50, 70, 90, and 100 °C [77, 122, 158, 194, and 230 °F] and Total Pressure Corresponding to $RH_{median}$ .....	2-9
2-7	Calculated $NO_3^-$ Concentrations of Brines Resulting From Evaporation of Yucca Mountain Unsaturated Zone Waters at 25, 50, 70, 90, and 100 °C [77, 122, 158, 194, and 230 °F] and Total Pressure Corresponding to $RH_{median}$ .....	2-10
2-8	Calculated $F^-$ Concentrations of Brines Resulting From Evaporation of Yucca Mountain Unsaturated Zone Waters at 25, 50, 70, 90, and 100 °C [77, 122, 158, 194, and 230 °F] and Total Pressure Corresponding to $RH_{median}$ .....	2-11
2-9	Calculated $SO_4^{2-}$ Concentrations of Brines Resulting From Evaporation of Yucca Mountain Unsaturated Zone Waters at 25, 50, 70, 90, and 100 °C [77, 122, 158, 194, and 230 °F] and Total Pressure Corresponding to $RH_{median}$ .....	2-12
2-10	Calculated $HCO_3^- + CO_3^{2-}$ Concentrations of Brines Resulting From Evaporation of Yucca Mountain Unsaturated Zone Waters at 25, 50, 70, 90, and 100 °C [77, 122, 158, 194, and 230 °F] and Total Pressure Corresponding to $RH_{median}$ .....	2-13
2-11	Calculated Ionic Strength (moles/kg $H_2O$ ) of Brines Resulting From Evaporation of Yucca Mountain Unsaturated Zone Waters at 25, 50, 70, 90, and 100 °C [77, 122, 158, 194, and 230 °F] and Total Pressure Corresponding to $RH_{median}$ .....	2-14
2-12	Calculated $NO_3^-/Cl^-$ Mole Ratios of Brines Resulting From Evaporation of Yucca Mountain Unsaturated Zone Waters at 25, 50, 70, 90, and 100 °C [77, 122, 158, 194, and 230 °F] and Total Pressure Corresponding to $RH_{median}$ .....	2-15
2-13	Calculated pHs of Brines Resulting From Evaporation of Yucca Mountain Unsaturated Zone Waters at 50, 70, 90, and 100 °C [122, 158, 194, and 230 °F] and Total Pressure Corresponding to $RH_{median}$ .....	2-16
2-14	Calculated $NO_3^-/Cl^-$ Mole Ratios of Brines Resulting From Evaporation of Yucca Mountain Unsaturated Zone Waters at 50, 70, 90, and 100 °C [122, 158, 194, and 230 °F] and Total Pressure Corresponding to $RH_{median}$ .....	2-17
3-1	Schematic of Curve Derived With the Monte Carlo Approach To Quantify $P(E_{corr} > E_{crev})$ .....	3-5
3-2	Probability of $E_{corr} > E_{crev}$ as a Function of pH, Chloride, and Nitrate Concentration and Temperature .....	3-6
3-3	Localized Corrosion Boundaries (Probability = 0.001) as a Function of Chloride and Nitrate Concentrations and Temperature .....	3-10

## FIGURES (continued)

### Figure Page

3-4	Range of Waste Package Temperatures Reproduced From DOE [2008,Figure 2.3.5-33(b)] .....	3-11
3-5	DOE Computation of the Probability of Localized Corrosion as a Function of the Drip Shield Failure Time.....	3-12

## TABLES

Table    Page

2-1	Values at Various Temperatures of Pure Water Vapor Pressure ( $p_{H_2O^\circ}$ ), Median Relative Humidity ( $RH_{median}$ ), Lower Bound Relative Humidity ( $RH_{lower-bound}$ ) and Total Pressure Corresponding to $RH_{median}$ or $RH_{lower-bound}$ .....	2-3
3-1	Mean, Standard Deviation, and Covariance Matrix for the Parameters $a_0$ Through $a_4$ .....	3-1
3-2	Mean, Standard Deviation, and Covariance Matrix for the Parameters $c_0$ Through $c_6$ .....	3-2

## ACKNOWLEDGMENTS

This report was prepared to document work performed by the Center for Nuclear Waste Regulatory Analyses (CNWRA<sup>®</sup>) for the U.S. Nuclear Regulatory Commission (USNRC) under Contract No. NRC-02-07-006. The activities reported here were performed on behalf of the USNRC Office of Nuclear Material Safety and Safeguards, Division of High-Level Waste Repository Safety. This report is an independent product of CNWRA and does not necessarily reflect the views or regulatory position of USNRC.

The authors wish to thank Xihua He for her technical review, Todd Mintz for his programmatic review, Lauren Mulverhill for her editorial review, and Arturo Ramos for his secretarial support.

## QUALITY OF DATA, ANALYSES, AND CODE DEVELOPMENT DATA

**DATA:** All CNWRA-generated data contained in this report meet quality assurance requirements described in the Geosciences and Engineering Division Quality Assurance Manual. Sources of other data should be consulted for determining the level of quality of those data.

**ANALYSES AND CODES:** This report includes results of calculations performed using Geochemist's Workbench<sup>®</sup> (Bethke and Yeakel, 2007) and OLI Analyzer Studio (OLI Systems, Inc., 2010)—commercially available software maintained in accordance with CNWRA Technical Operating Procedure (TOP)-018, Development and Control of Scientific and Engineering Software. Data reduction, probability computations, and plotting were accomplished using Microsoft<sup>®</sup> Excel<sup>®</sup> (Microsoft Corporation, 2002), Sigmaplot<sup>®</sup> (Systat Software, Inc., 2008), and Mathematica<sup>®</sup> (Wolfram Research, Inc., 2011). Work in this report related to the chemistry of solutions is documented in Scientific Notebook 930E (Pabalan, 2010).

## References

Bethke, C.M. and S. Yeakel. "Geochemist's Workbench<sup>®</sup> Release 7.0." Golden, Colorado: RockWare, Inc. 2007.

Microsoft Corporation. "Excel<sup>®</sup>." Redland, Washington: Microsoft Corporation. 2002.

OLI Systems, Inc. "A Guide to Using OLI Analyzer Studio Version 3.1." Morris Plains, New Jersey: OLI Systems, Inc. 2010.

Pabalan, R.T. "Quantity and Chemistry of Water Contacting Engineered Barriers Integrated Subissue." Scientific Notebook 930E. San Antonio, Texas: CNWRA. 2010.

Systat Software, Inc. "Sigmaplot<sup>®</sup> 11." San Jose, California: Systat Software, Inc. 2008.

Wolfram Research, Inc. "Mathematica<sup>®</sup>." Champaign, IL: Wolfram Research, Inc. 2011.

## 1 INTRODUCTION

This report is part of the knowledge management activities for the U.S. Nuclear Regulatory Commission high-level waste repository safety program. The report provides a previously undocumented methodology to estimate the likelihood of localized corrosion of waste package materials in repository settings. A key attribute of the U.S. Department of Energy (DOE) safety strategy for the high-level nuclear waste repository it had proposed to construct at Yucca Mountain, Nevada, was long-lived waste packages and drip shields (DOE, 2008). The waste packages were to consist of an outer container of a highly corrosion-resistant nickel–chromium–molybdenum alloy (Alloy 22) over an inner container made of Type 316 nuclear grade stainless steel. Arched drip shields made of a titanium–palladium alloy (Titanium Grade 7) were to extend over the length of the emplacement drifts to cover the waste packages and protect them against seepage water and rockfall arising from gradual drift degradation. However, seepage water could contact the waste package if drip shields were breached by some mechanism (e.g., due to rock loads arising from drift degradation and seismic activity). In the absence of mechanical disruption, DOE expected aqueous corrosion to be the primary degradation process limiting the life of the waste packages and drip shields.

The mode and rate of corrosion of the waste package and drip material materials were expected to depend on the chemistry of water contacting them and on temperature. Coupled thermal-hydrological-chemical processes would significantly alter the chemistry of groundwater that seeps into the repository drift and contacts the waste packages and drip shields. Radioactive decay can cause waste packages and drip shields to experience transient temperatures above the boiling point of pure water for several hundreds to few thousands of years. During this transient elevated temperature period, seepage water evaporation could lead to the formation of corrosive brines on waste package and drip shield surfaces.

This report documents a methodology to evaluate the likelihood of environmental conditions capable of supporting initiation of localized corrosion of the Alloy 22 waste package material due to seepage water evaporation. Another source of water that could enable corrosion processes (i.e., the deliquescence of salts present in dusts deposited on the waste package or drip shield surface) was considered in a separate evaluation (e.g., Yang, et al., 2011). The approach presented in this report accounts for the variability in solution composition, pH, and temperature of the Alloy 22 material. The method is based on the concept of corrosion and repassivation potentials and their dependence on the chemistry of brines that may evolve from seepage water evaporation.

This report has two main chapters. In Chapter 2, the potential chemistry of solutions in contact with waste package and drip shield materials is evaluated based on independent thermodynamic simulations. As indicated in a preceding paragraph, seepage water chemistry will evolve due to evaporation during the transient elevated temperature period. The chemistry of solutions that eventually contact the waste packages and drip shields is a function of the initial water composition (i.e., composition of seepage water), air pressure and water content in air (i.e., relative humidity), and the temperature of the EBS materials that the solutions are postulated to contact. In Chapter 3, the DOE equations for the computation of corrosion and repassivation potentials are examined. The range of chemical compositions from Chapter 2 is used as input to define conditions under which localized corrosion could arise. Factors controlling the <12,000-year localized corrosion window DOE established also are discussed in Chapter 3.



## 2 CHEMISTRY OF SOLUTIONS CONTACTING WASTE PACKAGES AND DRIP SHIELDS

The approach to estimate the compositions of solutions that could contact the waste packages and drip shields is described as follows. The composition of seepage water is assumed to be similar to Yucca Mountain unsaturated zone groundwaters. The Yucca Mountain unsaturated zone contains pore water, fracture water, and isolated lenses of perched water. Yang, et al. (2003, 1998, 1996) measured the chemical compositions of pore water and perched water from Yucca Mountain. Perched waters were sampled from boreholes using plastic bailers, and pore waters were extracted from borehole core samples using high-pressure uniaxial compression techniques. Although there are significant uncertainties in the pore water chemistry data resulting from the air drilling of core samples, pore water evaporation, and the compression techniques (Yang, et al., 2003, 1998, 1996; Browning, et al., 2000), they provide a valuable characterization of Yucca Mountain groundwater chemistry. No measured compositions of Yucca Mountain fracture waters are available because these waters are hard to sample. However, samples of fracture water have been collected at Rainier Mesa, which is located about 50 km [31 mi] north-northeast of Yucca Mountain, and those are similar in composition to perched and saturated zone waters collected at Yucca Mountain. The saturated zone groundwaters lie below the proposed repository site, and their compositions were not considered in this evaluation, although DOE has extensively used samples of this water, pumped from the J-13 Well, to define a reference Yucca Mountain groundwater composition for experimental studies (e.g., Rosenberg, et al., 1999, 2001).

For the analysis and for the sake of efficiency, 33 Yucca Mountain unsaturated zone pore water compositions were selected from the 156 unsaturated zone compositions available from the Yang, et al. (2003, 1998, 1996) compilation. Most of the 156 compositions correspond to pore water samples, and a few correspond to perched water samples, which were included to expand the range in water chemistry considered in the analysis. The 33 samples were selected to represent the range and distribution of the water compositions in the data set and the 3 brine types—calcium chloride, alkaline, and neutral—that could result from evaporation.<sup>1</sup> Eleven compositions from each water type were used in the analysis. The water compositions in the dataset are depicted in a ternary diagram in Figure 2-1.

Thermodynamic simulations were conducted to determine the chemical evolution of in-drift waters resulting from evaporation. The thermodynamic calculations used the OLI Analyzer Studio Version 3 code (Gerbino, 2006; OLI Systems, Inc., 2010). The code, using its mixed-solvent electrolyte chemistry option, allows for simulation of aqueous chemical systems for temperatures up to 300 °C [572 °F], pressures up to 1,500 bar, and concentrations ranging from dilute conditions to the pure molten salts or pure acids. Thermodynamic properties calculated with this software have been shown to agree very well with experimental data (e.g., Gruskiewicz, et al., 2007).

---

<sup>1</sup>In natural systems, the chemical evolution of evaporating water generally is controlled by the high solubility of salt minerals relative to the moderate solubility of calcium sulfate and the low solubility of calcium carbonate minerals—a mechanism referred to as chemical divide (Hardie and Eugster, 1970). Thus, evaporation of initially dilute natural waters at the Earth's surface, such as in saline lakes, typically leads to the formation of three brine types: calcium chloride brine, alkaline carbonate brine, and high sulfate (also referred to as “neutral”) brine (Spencer, 2000). The same brine types could occur within the drifts because in-drift brines are produced by processes similar to those that occur at the Earth's surface.

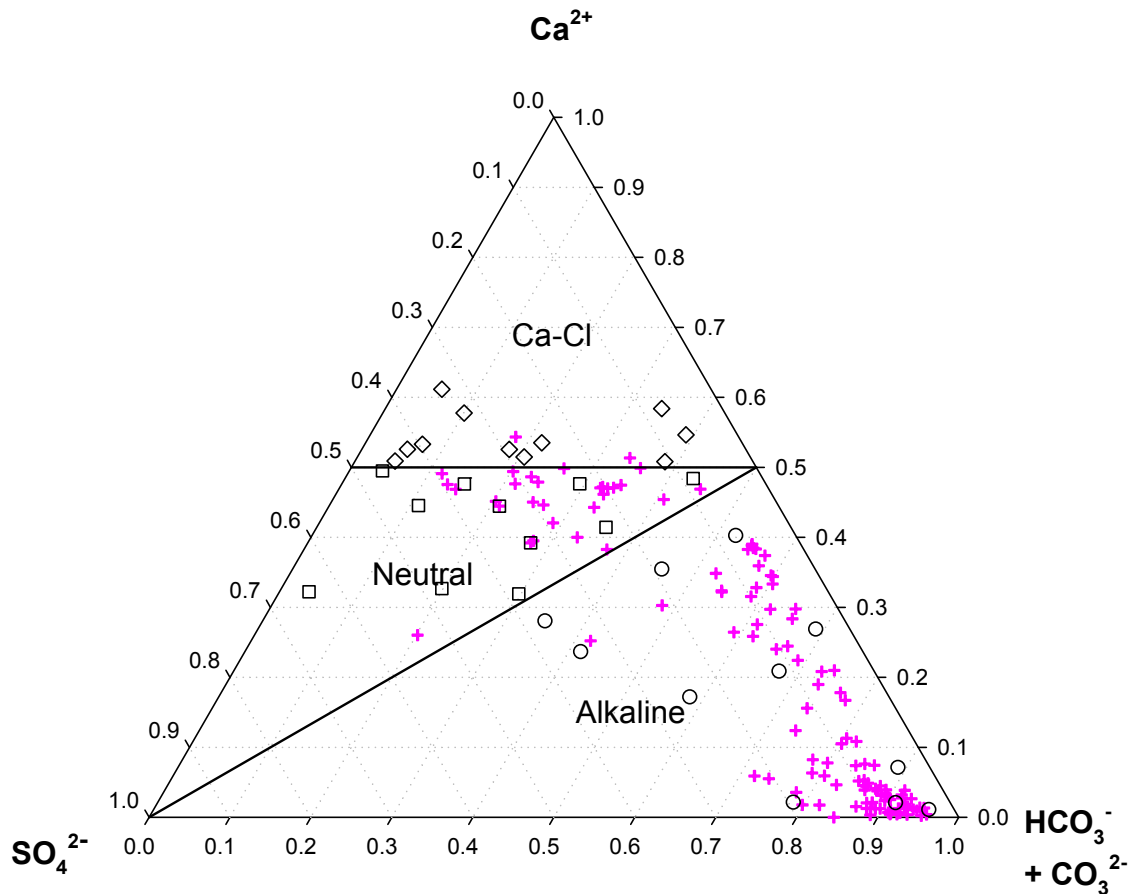


**Figure 2-1. Composition of Yucca Mountain Unsaturated Zone Waters. Circles, Squares, and Diamonds Represent the Compositions of Alkaline-, Neutral-, and Calcium-Chloride-Type Waters That Were Used as Input to Thermodynamic Evaporation Simulations. All the Other Data Were Considered in Determining the Frequency of the Three Brine Types Based on the Chemical Divide Concept. Water Composition Data Are From Yang, et al. (2003, 1998, 1996).**

Prior to running the evaporation simulations using OLI Analyzer, the analytical data were input into Geochemist's Workbench REACT Version 7.0 and charge balanced. The REACT calculations followed the Browning, et al. (2000) approach, which constrained the carbonate species by assuming equilibrium with a  $\text{CO}_2(\text{g})$  fugacity equal to  $10^{-2.991}$  and set  $\text{O}_2(\text{g})$  fugacity to 0.7706 atm. REACT was used for the initial calculations because OLI Analyzer does not have an option for fixing gas fugacities at specified values. In contrast to the Browning, et al. (2000) approach, which set the  $\text{K}^+$  concentration to 14 mg/L when the published chemical analysis did not have a value for  $\text{K}^+$ , a value of zero was used in REACT if no  $\text{K}^+$  value was reported. Also, Browning, et al. (2000) did not include  $\text{F}^-$  in their study. In the evaluation described in this report,  $\text{F}^-$  was included in the input file to enable an assessment, discussed in the Technical Evaluation Report, of the potential effect of seepage water evaporation on titanium drip shield corrosion. An  $\text{F}^-$  concentration of 2.18 mg/L, which is an average value for

J-13 well waters Harrar, et al. (1990) reported, was used in the REACT calculations if no value was reported in the Yang, et al. (2003, 1998, 1996) compilation.

The REACT output values of  $\text{Na}^+$ ,  $\text{K}^+$ ,  $\text{Mg}^{2+}$ ,  $\text{Ca}^{2+}$ ,  $\text{Cl}^-$ ,  $\text{NO}_3^-$ ,  $\text{F}^-$ ,  $\text{HCO}_3^-$ ,  $\text{SO}_4^{2-}$ , and  $\text{SiO}_2(\text{aq})$  for each of the 33 water samples were input into OLI Analyzer, and evaporation simulation was conducted. The OLI Analyzer calculations were done isothermally at 25, 50, 70, 90, and 110 °C [77, 122, 158, 194, and 230 °F]. At each temperature, the total pressure,  $P_{\text{total}}$ , specified for each OLI Analyzer isothermal calculation was derived from the following equation

$$P_{\text{total}} = RH_{\text{median}} \times p_{\text{H}_2\text{O}}(T_{\text{WP}}) \quad (2-1)$$

where  $RH_{\text{median}}$  is a calculated median relative humidity at the waste package surface and  $p_{\text{H}_2\text{O}}$  is the equilibrium vapor pressure of pure water at the waste package surface temperature ( $T_{\text{WP}}$ ).  $P_{\text{total}}$  corresponds to the vapor pressure of the concentrated aqueous solution at equilibrium. In other words, the OLI Analyzer calculation proceeds along an increasing degree of evaporation until the calculated vapor pressure of solution becomes equal to  $P_{\text{total}}$ . To derive  $RH_{\text{median}}$ , the waste package surface relative humidity was determined from data derived from the Total-system Performance Assessment (TPA) code (Leslie, et al., 2007), which was executed in Monte Carlo mode to account for uncertainty in thermohydrological rock features. This code was used to compute the waste package temperature and relative humidity as functions of time, and from these data the median and bounding values were derived. Uncertainty in the relative humidity at the waste package surface is the result of spatial variability and uncertainty in thermohydrological rock features (Manepally and Fedors, 2003). Values of  $RH_{\text{median}}$ ,  $p_{\text{H}_2\text{O}}$ , and  $P_{\text{total}}$  as a function of temperature are listed in Table 2-1. The  $RH_{\text{median}}$  value at 25 °C [77 °F] was assumed to be 1.0. Note that only median values of the relative humidity were used in the analyses discussed in Chapter 3 of this report. However, to determine the possible effect of lower relative humidity on the calculated solution chemistry, additional calculations were done at the lower bounding relative humidity ( $RH_{\text{lower-bound}}$ ) determined from the TPA code for temperatures of 50, 70, 90, and 110 °C [122, 158, 194, and 230 °F].  $RH_{\text{lower-bound}}$  values used in the calculations are also listed in Table 2-1.

In some OLI Analyzer runs, particularly at 90 and 110 °C [194 and 230 °F], using the relative humidity values listed in Table 2-1 caused the solution to completely evaporate. In those cases, the total pressure specified in the OLI Analyzer input was increased slightly such that the equilibrium solution composition retained some amount of aqueous phase.

<b>Table 2-1. Values at Various Temperatures of Pure Water Vapor Pressure (<math>p_{\text{H}_2\text{O}}</math>), Median Relative Humidity (<math>RH_{\text{median}}</math>), Lower Bound Relative Humidity (<math>RH_{\text{lower-bound}}</math>), and Total Pressure Corresponding to <math>RH_{\text{median}}</math> or <math>RH_{\text{lower-bound}}</math>. <math>P_{\text{total}}</math> Was Used as Input in the OLI Analyzer Calculations.</b>					
$T_{\text{WP}}$	$p_{\text{H}_2\text{O}}$	$RH_{\text{median}}$	$P_{\text{total}}$ (atm) Corresponding to $RH_{\text{median}}$	$RH_{\text{lower-bound}}$	$P_{\text{total}}$ (atm) Corresponding to $RH_{\text{lower-bound}}$
25 °C [77 °F]	0.031385	1.0	0.031385	—	—
50 °C [122 °F]	0.12207	0.724841	0.088481	0.597626	0.072952
70 °C [158 °F]	0.307827	0.618355	0.190346	0.450068	0.138543
90 °C [194 °F]	0.69101	0.549577	0.379763	0.367668	0.254062
110 °C [230 °F]	1.40854	0.45498	0.640858	0.303936	0.428106

The OLI Analyzer simulations allowed determination of the composition ranges of the three brine types (calcium chloride, alkaline, neutral) that may form in the emplacement drifts. Figures 2-2 to 2-12 show the results calculated at various temperatures using  $RH_{median}$  values. Figure 2-2 shows the calculated pH ranges for the three brine types, whereas Figures 2-3 to 2-10 show the calculated concentration ranges of  $Na^+$ ,  $Mg^{2+}$ ,  $Ca^{2+}$ ,  $Cl^-$ ,  $NO_3^-$ ,  $F^-$ ,  $SO_4^{2-}$ , and  $[HCO_3^- + CO_3^{2-}]$ . Figures 2-11 and 2-12 show the calculated ionic strength and  $NO_3^-/Cl^-$  mole ratio, respectively, for the three brine types at various temperatures. The calculated ranges of pH and  $NO_3^-/Cl^-$  mole ratio at 50, 70, 90, and 110 °C [122, 158, 194, and 230 °F] using  $RH_{lower-bound}$  values are shown in Figures 2-13 and 2-14.

To provide a basis for estimating the range of solution compositions for the three brine types, the full set of Yang, et al. (2003, 1998, 1996) unsaturated zone water chemistry data was used jointly with the Hardie and Eugster (1970) chemical divide concept. Of the 156 compositions (all depicted in Figure 2-1), 8, 24, and 68 percent form calcium-chloride-, neutral-, and alkaline-type brines, respectively.

The plots in Figures 2-2 to 2-14 define a reasonable range of solution compositions that could arise in case seepage water evaporated and formed a solution in contact with EBS materials, such as titanium drip shields or Alloy 22 waste packages. The ranges of solution compositions in Figures 2-2 to 2-14 are presented in the form of box and whiskers plots. In these plots, the left and right sides of each box are the 25<sup>th</sup> and 75<sup>th</sup> percentiles, and the line inside the box is the median value. The whiskers are the 10<sup>th</sup> and 90<sup>th</sup> percentiles, and the points beyond the whiskers are outliers. The solution compositions were derived assuming thermodynamic equilibrium is achieved. This is an important point that merits additional discussion. If seepage water accumulated, for example, on the waste package surface, the solution would evaporate and evolve toward a solution composition with a water pressure in equilibrium with the environmental water pressure. If the relative humidity was low, the solution would evolve toward a concentrated system (i.e., a system of low water activity). Conversely, if the relative humidity was high, the solution would evolve toward a diluted system (i.e., a system of high water activity). In the analysis presented in this report, the relative humidity is assumed controlled by the temperature of the drift wall (the drift wall rock is assumed water saturated) and the temperature of the waste package surface. For a given waste package temperature, using the TPA Code Version 5.1, a range of reasonable relative humidities was estimated. It is reasonable to assume that the relative humidity is an independent variable that controls the equilibrium solution composition.

The range of water chemistries shown in Figures 2-2 to 2-14 are considered in Chapter 3 to establish whether solutions could arise that could lead to localized corrosion of Alloy 22. The relative humidity value adopted in the localized corrosion evaluation discussed in Chapter 3 is the median value shown in Table 2-1, although the effect of lower relative humidity causing a decrease in solution pH (e.g., compare Figure 2-13 with Figure 2-2) also is considered.

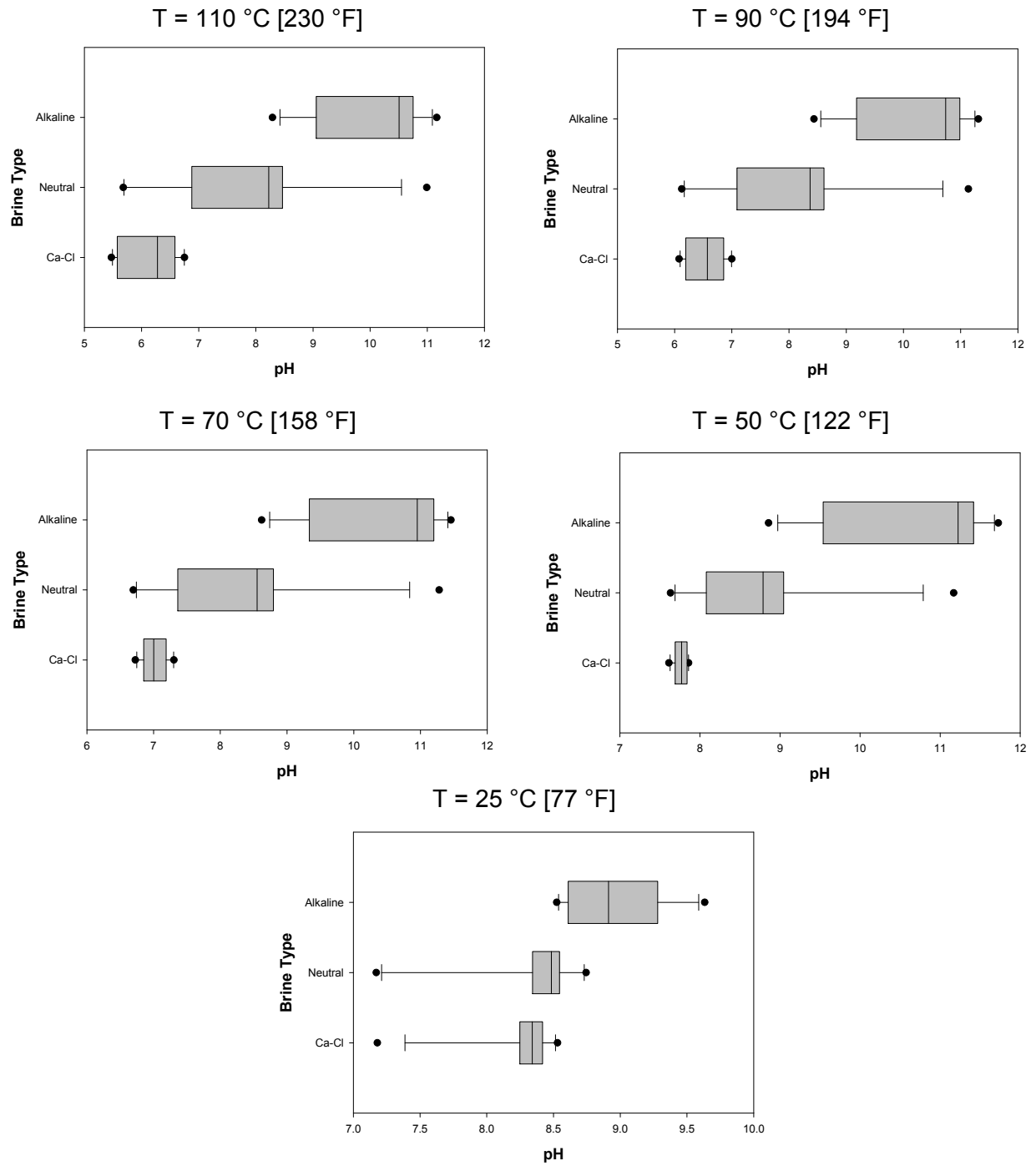


**Figure 2-2. Calculated pHs of Brines Resulting From Evaporation of Yucca Mountain Unsaturated Zone Waters at 25, 50, 70, 90, and 110 °C [77, 122, 158, 194, and 230 °F] and Total Pressure Corresponding to  $RH_{median}$ . In the Box Plots Shown in Figures 2-2 to 2-14, the Left and Right Sides of Each Box Are the 25<sup>th</sup> and 75<sup>th</sup> Percentiles, Respectively, and the Line Inside the Box Is the Median Value. The Whiskers Are the 90<sup>th</sup> and 10<sup>th</sup> Percentiles, and the Solid Circles Are Outliers.**

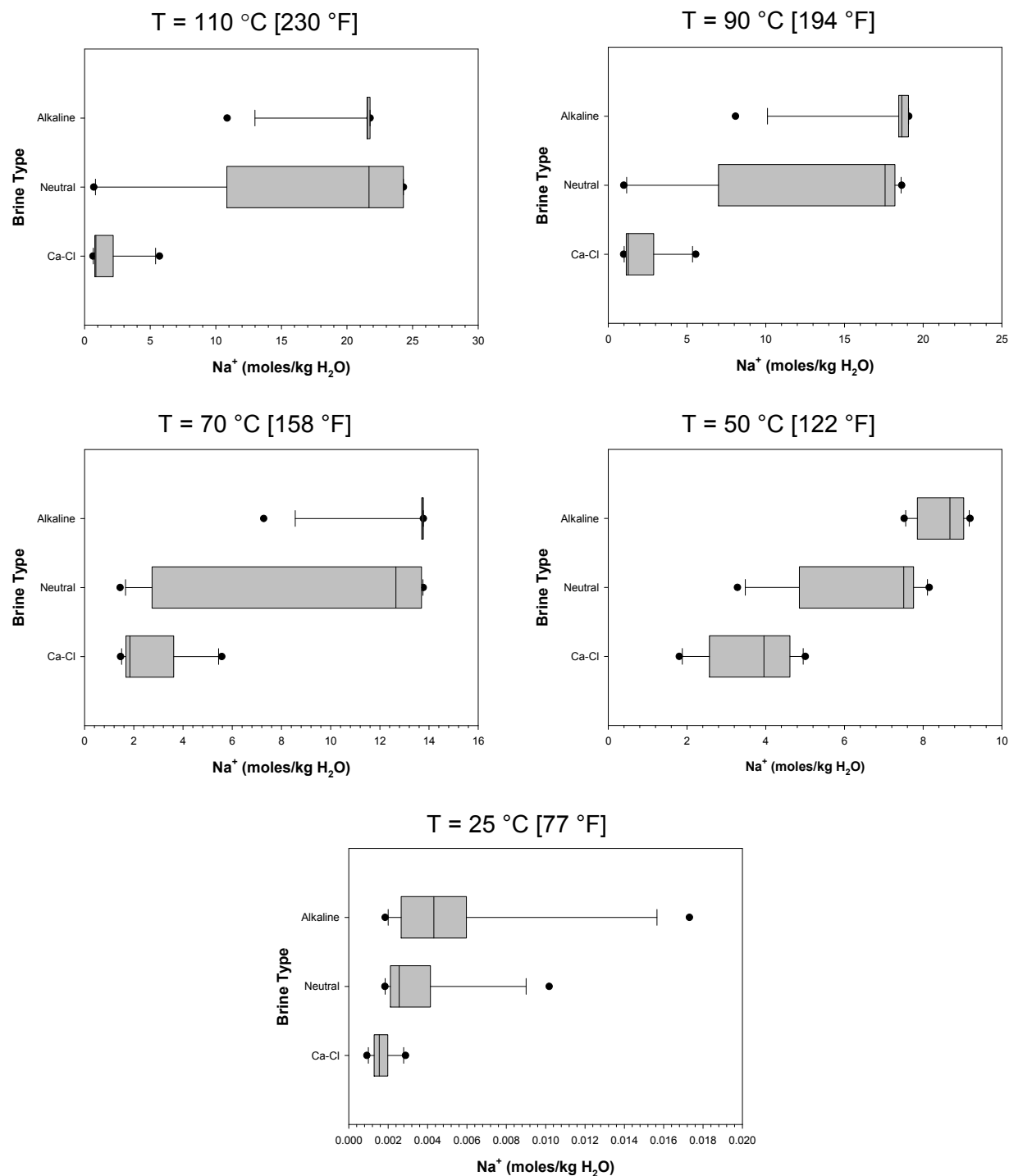


**Figure 2-3. Calculated  $\text{Na}^+$  Concentrations of Brines Resulting From Evaporation of Yucca Mountain Unsaturated Zone Waters at 25, 50, 70, 90, and 110 °C [77, 122, 158, 194, and 230 °F] and Total Pressure Corresponding to  $RH_{\text{median}}$**

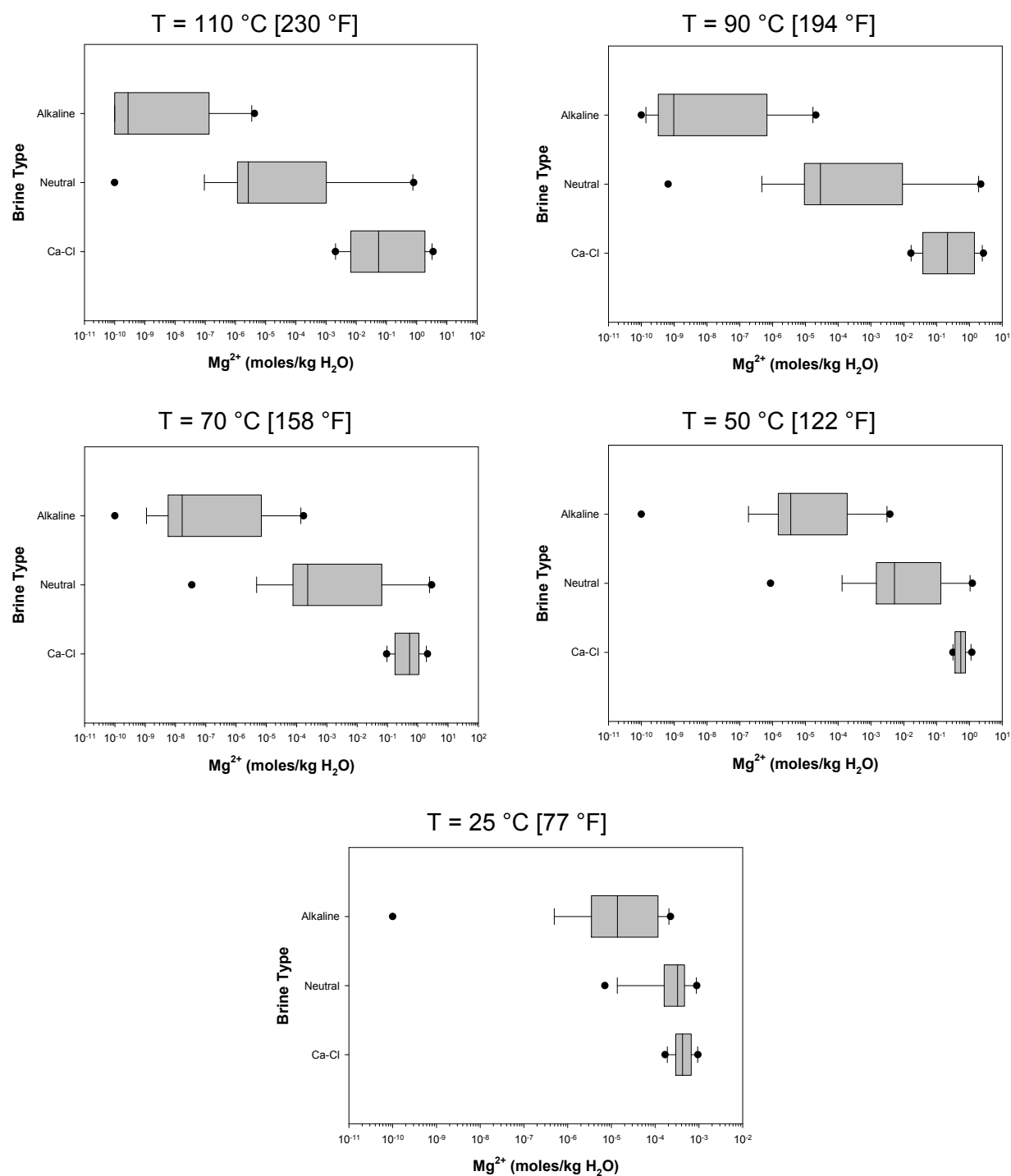


**Figure 2-4. Calculated  $Mg^{2+}$  Concentrations of Brines Resulting From Evaporation of Yucca Mountain Unsaturated Zone Waters at 25, 50, 70, 90, and 110 °C [77, 122, 158, 194, and 230 °F] and Total Pressure Corresponding to  $RH_{median}$**

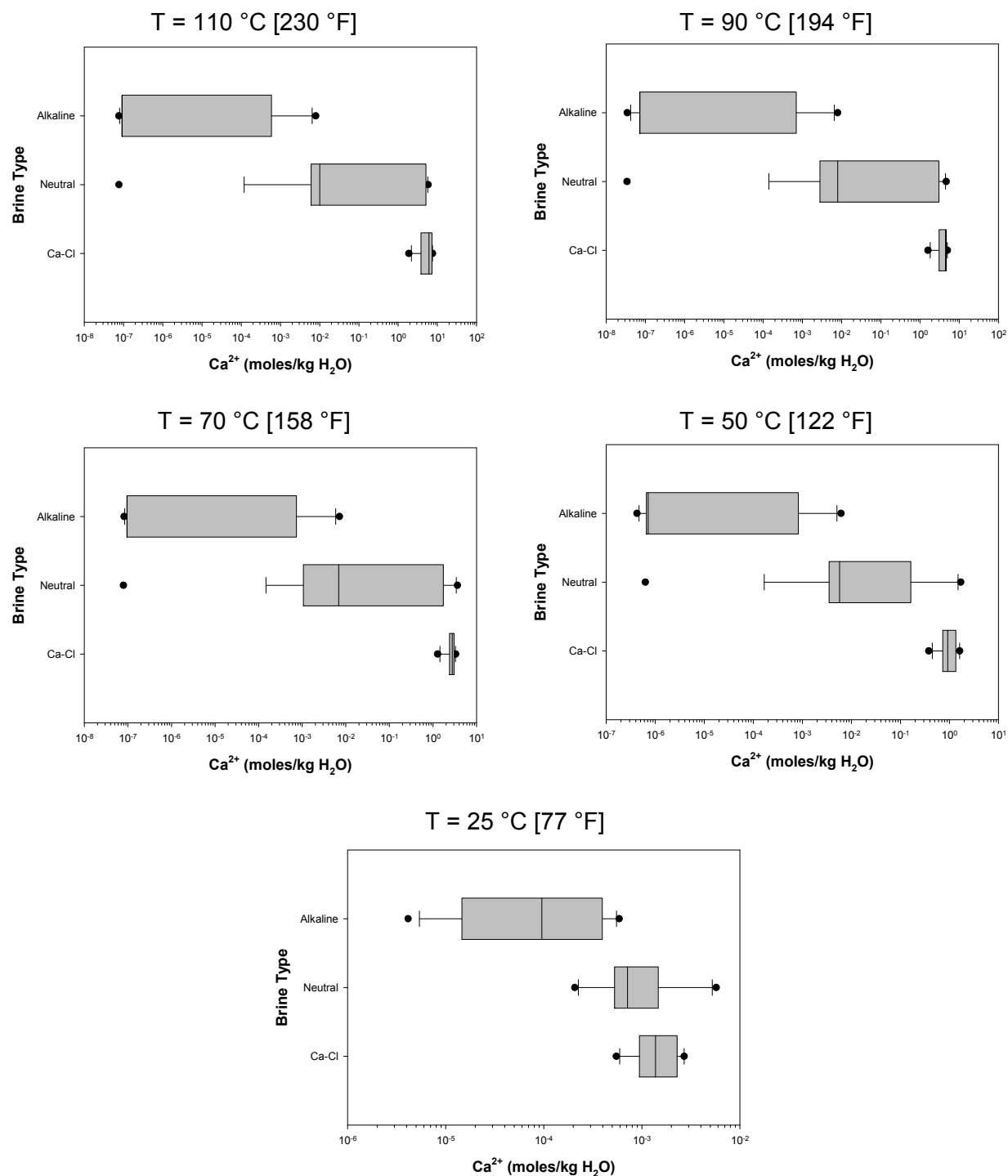


**Figure 2-5. Calculated  $\text{Ca}^{2+}$  Concentrations of Brines Resulting From Evaporation of Yucca Mountain Unsaturated Zone Waters at 25, 50, 70, 90, and 110 °C [77, 122, 158, 194, and 230 °F] and Total Pressure Corresponding to  $RH_{\text{median}}$**



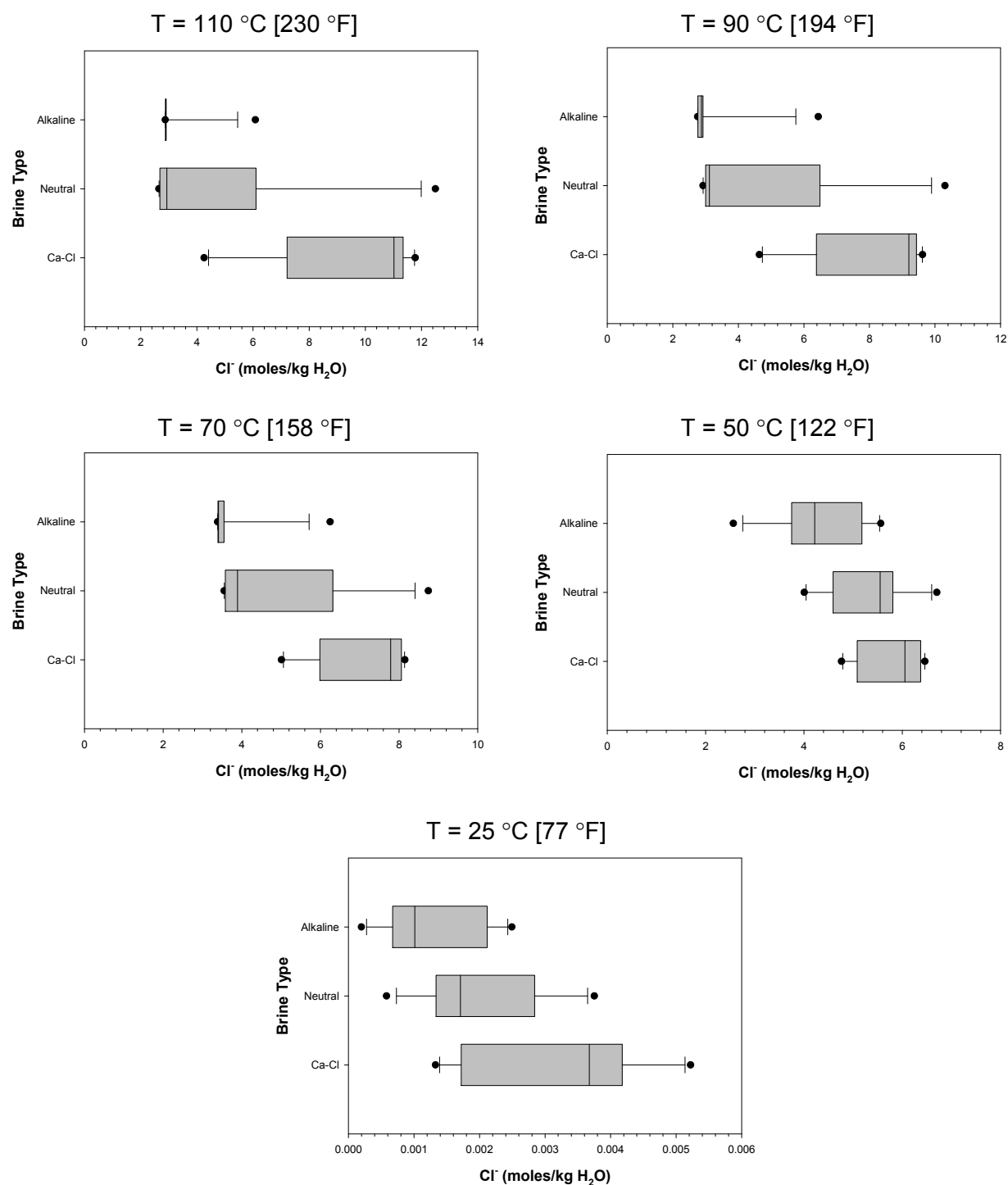


**Figure 2-6. Calculated  $\text{Cl}^-$  Concentrations of Brines Resulting From Evaporation of Yucca Mountain Unsaturated Zone Waters at 25, 50, 70, 90, and 110 °C [77, 122, 158, 194, and 230 °F] and Total Pressure Corresponding to  $RH_{\text{median}}$**

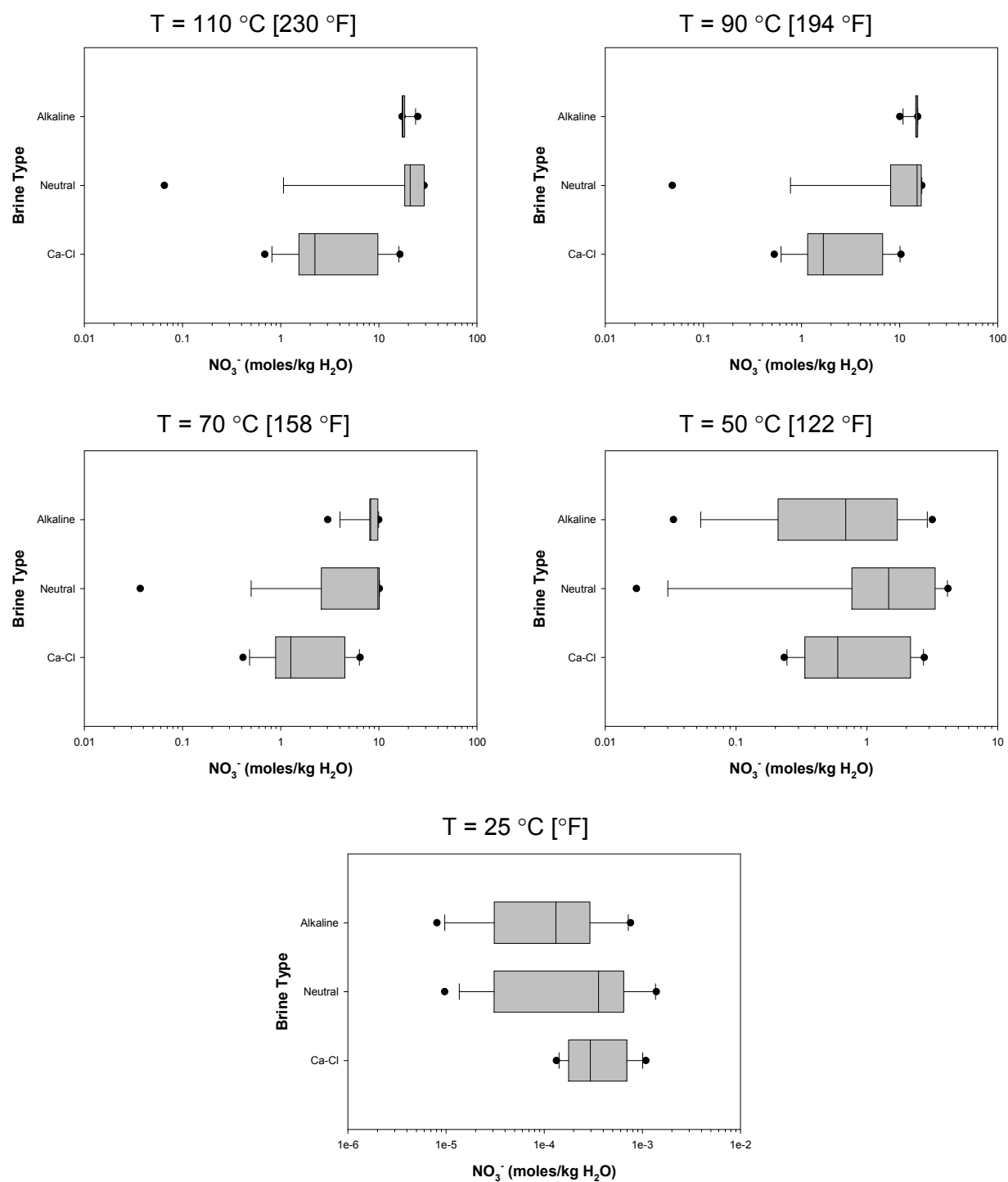


**Figure 2-7. Calculated  $\text{NO}_3^-$  Concentrations of Brines Resulting From Evaporation of Yucca Mountain Unsaturated Zone Waters at 25, 50, 70, 90, and 110 °C [77, 122, 158, 194, and 230 °F] and Total Pressure Corresponding to  $RH_{\text{median}}$**

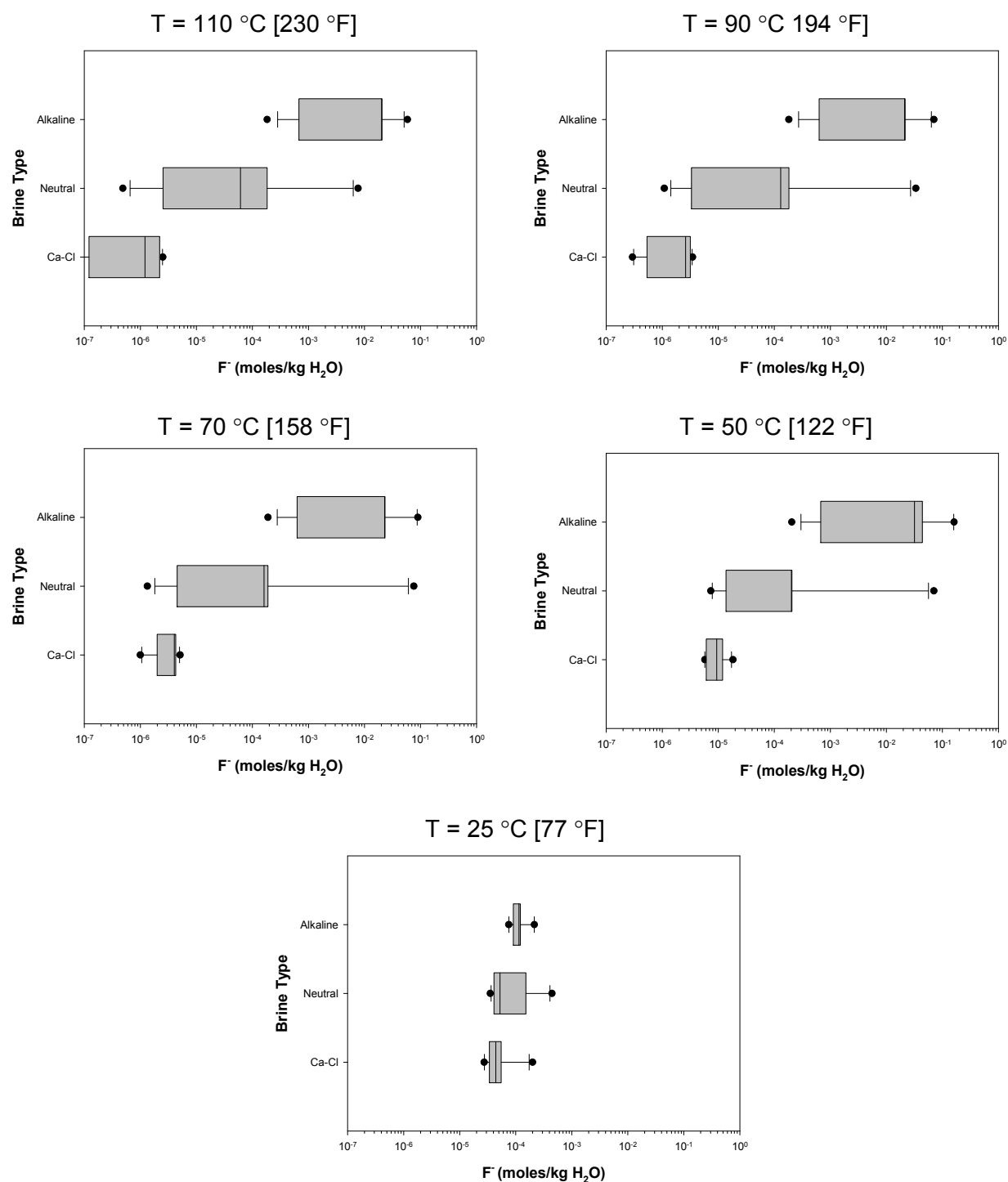


**Figure 2-8. Calculated  $F^-$  Concentrations of Brines Resulting From Evaporation of Yucca Mountain Unsaturated Zone Waters at 25, 50, 70, 90, and 110 °C [77, 122, 158, 194, and 230 °F] and Total Pressure Corresponding to  $RH_{median}$**

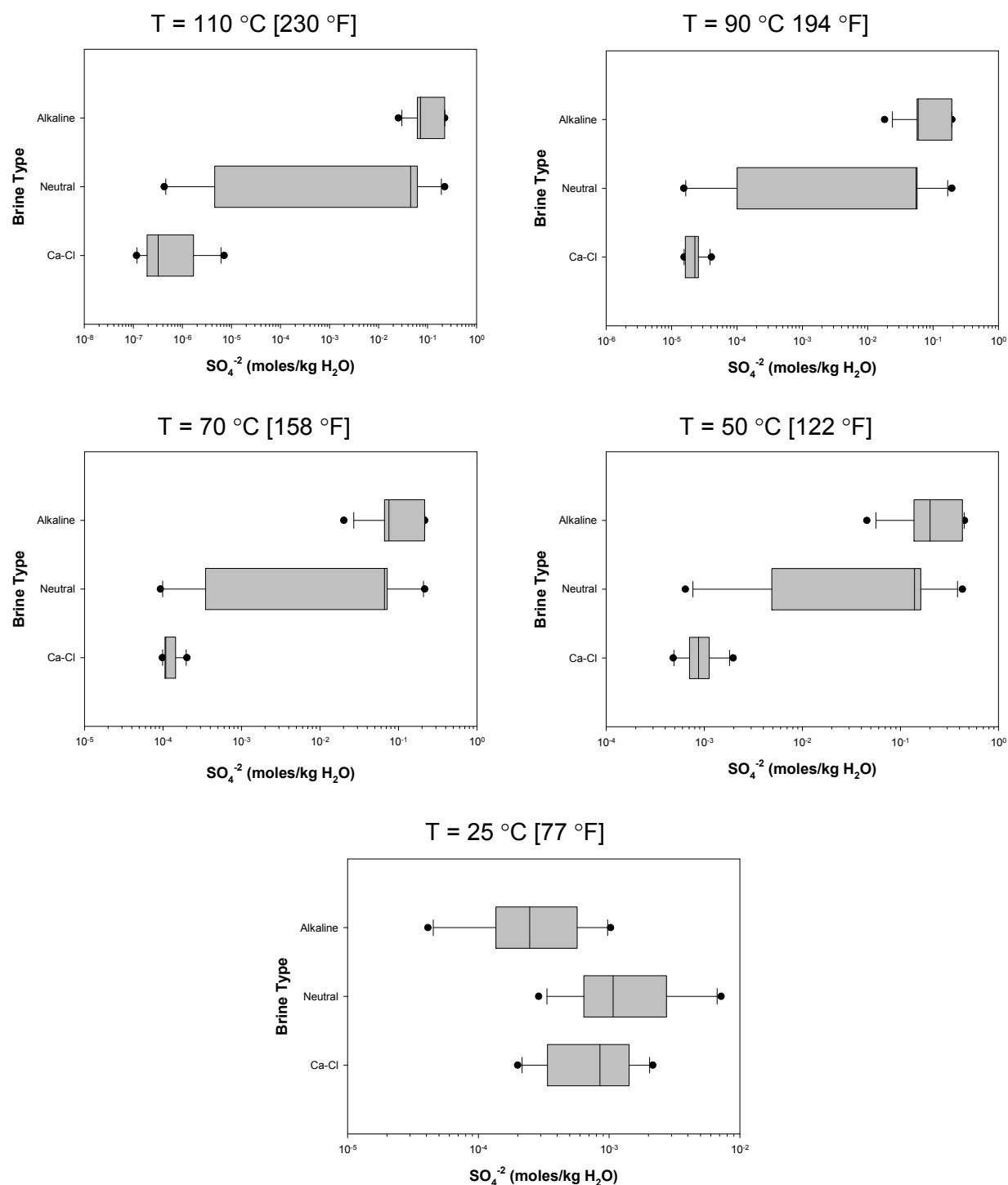


**Figure 2-9. Calculated  $\text{SO}_4^{2-}$  Concentrations of Brines Resulting From Evaporation of Yucca Mountain Unsaturated Zone Waters at 25, 50, 70, 90, and 110 °C [77, 122, 158, 194, and 230 °F] and Total Pressure Corresponding to  $RH_{\text{median}}$**

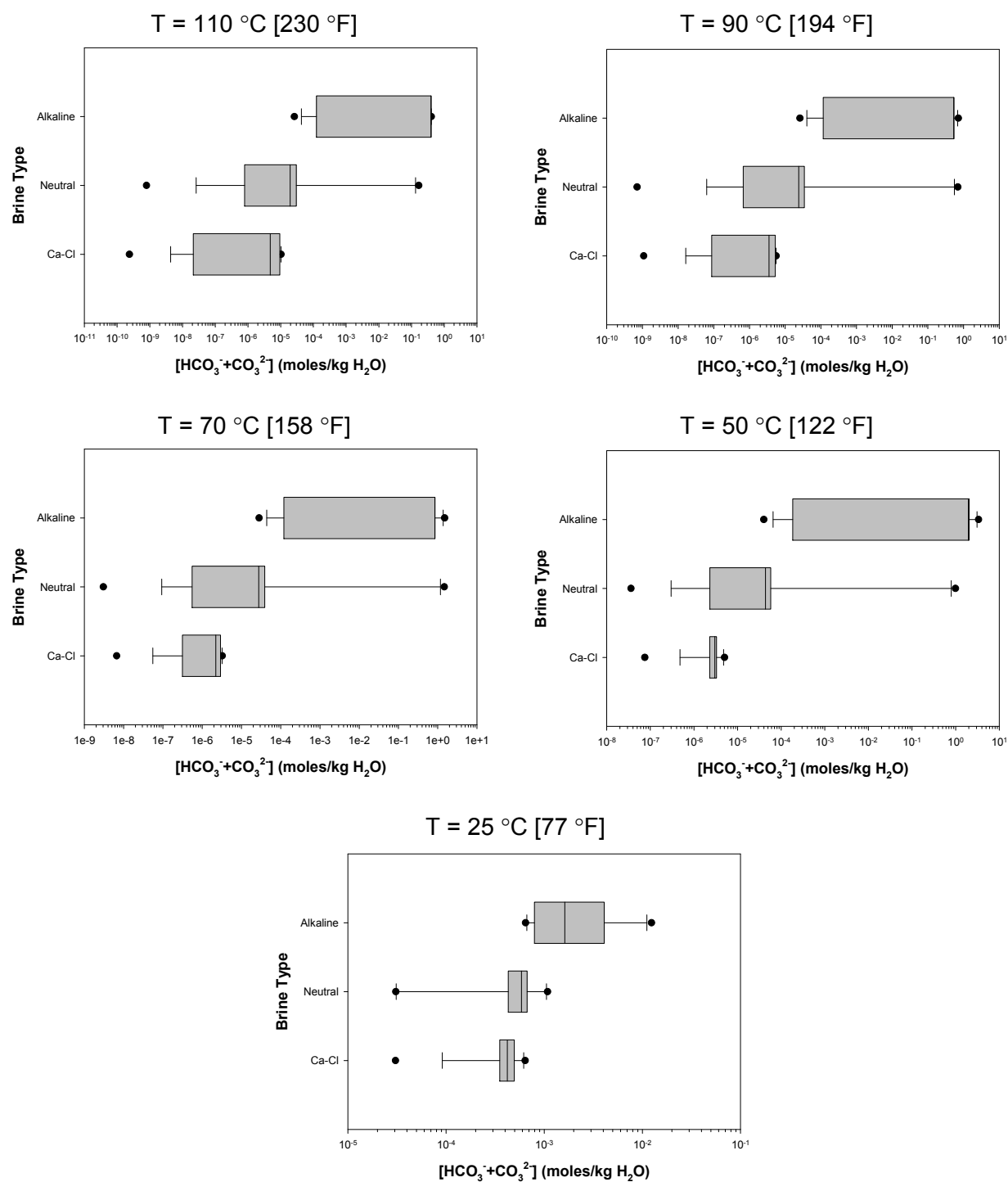


**Figure 2-10. Calculated  $\text{HCO}_3^- + \text{CO}_3^{2-}$  Concentrations of Brines Resulting From Evaporation of Yucca Mountain Unsaturated Zone Waters at 25, 50, 70, 90, and 110 °C [77, 122, 158, 194, and 230 °F] and Total Pressure Corresponding to  $RH_{\text{median}}$**

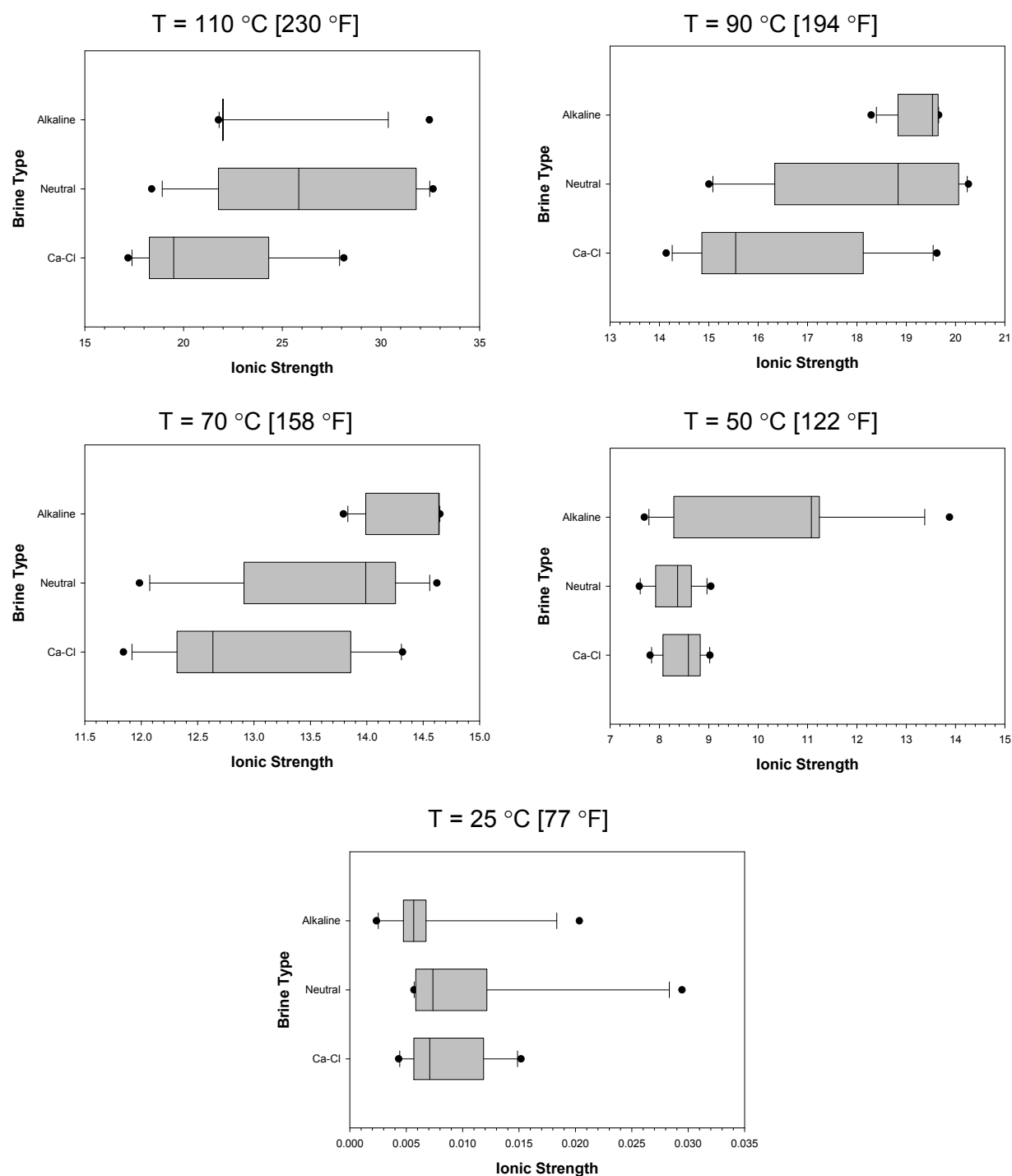


**Figure 2-11. Calculated Ionic Strength (moles/kg H<sub>2</sub>O) of Brines Resulting From Evaporation of Yucca Mountain Unsaturated Zone Waters at 25, 50, 70, 90, and 110 °C [77, 122, 158, 194, and 230 °F] and Total Pressure Corresponding to  $RH_{median}$**

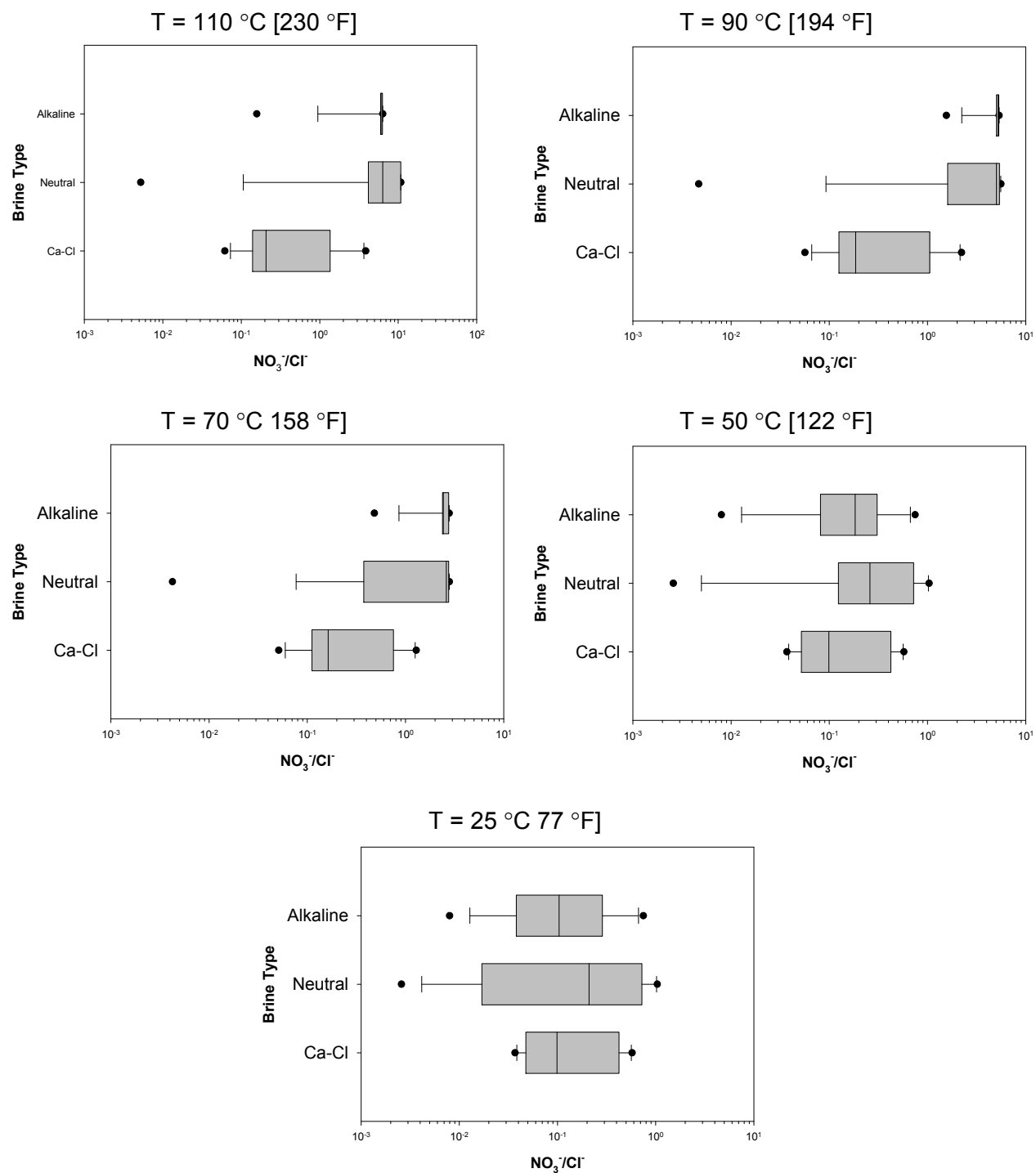


**Figure 2-12. Calculated  $\text{NO}_3^-/\text{Cl}^-$  Mole Ratios of Brines Resulting From Evaporation of Yucca Mountain Unsaturated Zone Waters at 25, 50, 70, 90, and 110 °C [77, 122, 158, 194, and 230 °F] and Total Pressure Corresponding to  $RH_{\text{median}}$**

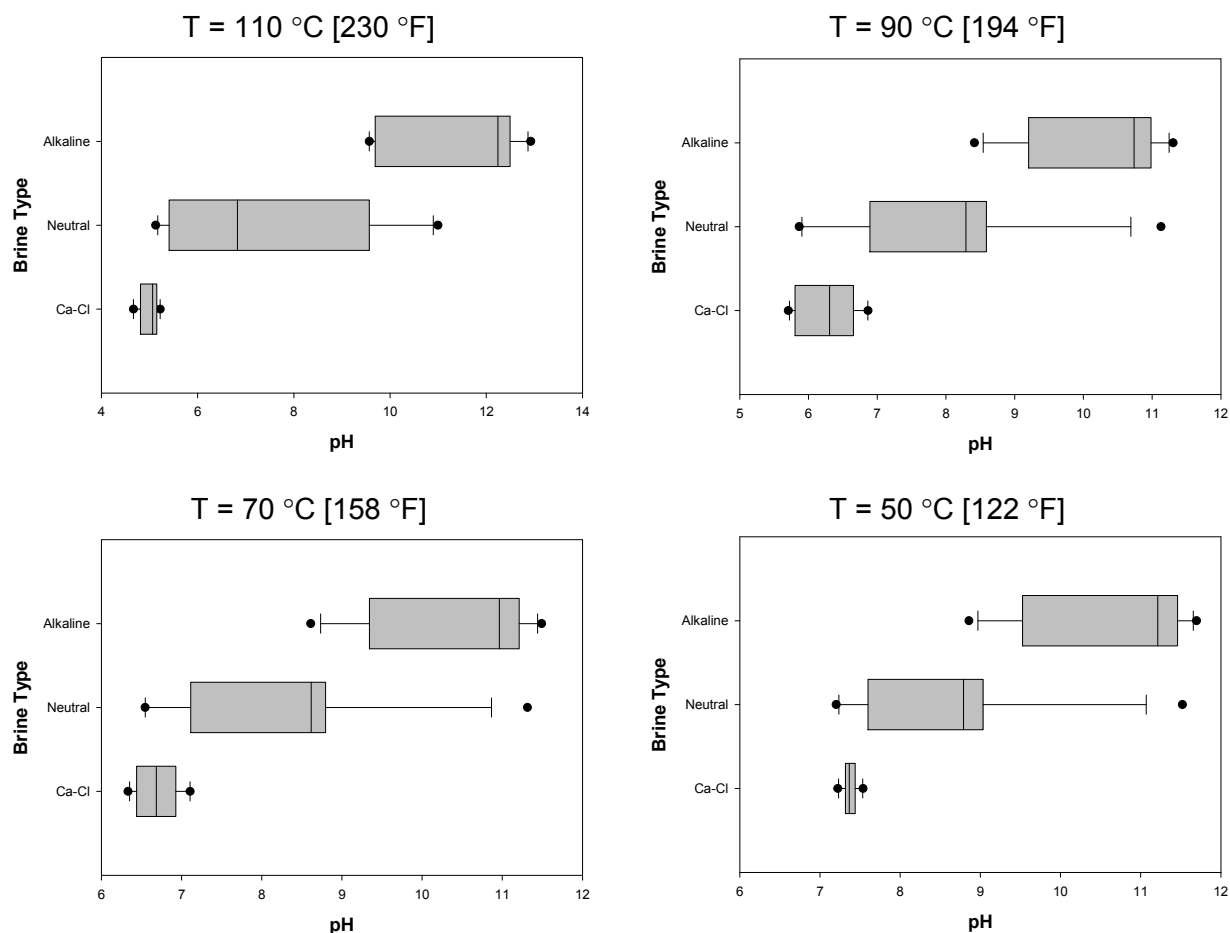


**Figure 2-13. Calculated pHs of Brines Resulting From Evaporation of Yucca Mountain Unsaturated Zone Waters at 50, 70, 90, and 110 °C [122, 158, 194, and 230 °F] and Total Pressure Corresponding to  $RH_{lower-bound}$**

In the DOE localized corrosion model for Alloy 22 described in Chapter 3, key electric potential equations are defined as functions of temperature, pH, chloride concentration, and nitrate-to-chloride ratio. The effect of other oxyanions, such as sulfate and carbonate, was ignored in the model. This approach is reasonable because these anions are known localized corrosion inhibitors (e.g., Pensado and Pabalan, 2008). Ignoring their presence in a corrosion model would tend to overestimate the frequency of localized corrosion.



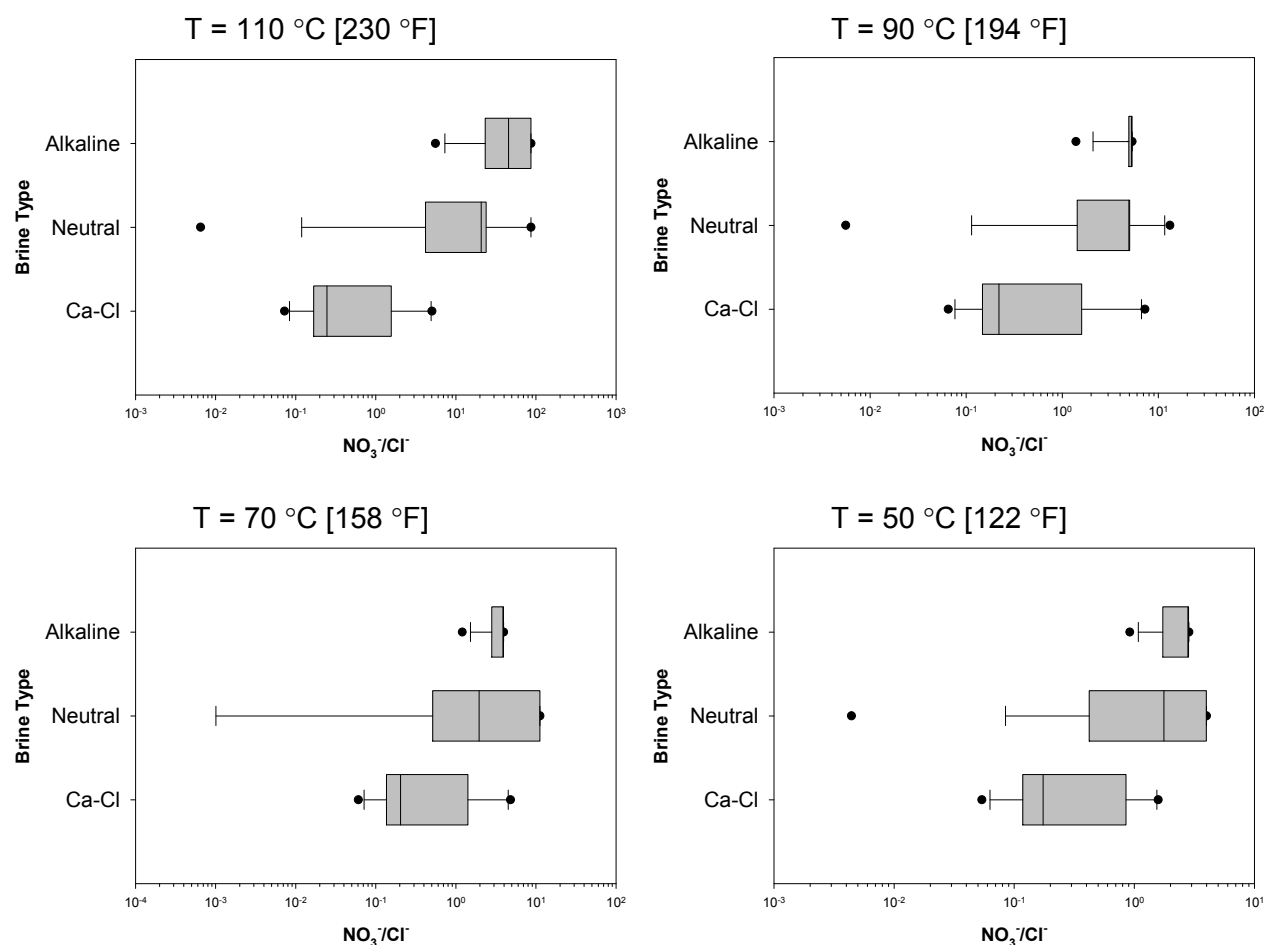


**Figure 2-14. Calculated  $\text{NO}_3^-/\text{Cl}^-$  Mole Ratios of Brines Resulting From Evaporation of Yucca Mountain Unsaturated Zone Waters at 50, 70, 90, and 110 °C [122, 158, 194, and 230 °F] and Total Pressure Corresponding to  $RH_{\text{lower-bound}}$**

### 3 ASSESSMENT OF DOE LOCALIZED CORROSION MODEL

In this chapter the U.S. Department of Energy (DOE) model for the initiation of localized corrosion in Alloy 22 as a function of the chemical composition of waters in a Yucca Mountain geological repository setting is analyzed (SNL, 2007). DOE concluded that localized corrosion of waste packages made of Alloy 22 is unlikely if the drip shield protects the waste package from seepage during at least 12,000 years (DOE, 2009a, Enclosure 1). This report presents a methodology to estimate the likelihood of localized corrosion of waste package materials using the equations DOE developed for corrosion potential and critical potentials. DOE adopted a critical potential approach to identify conditions that could lead to localized corrosion in Alloy 22. DOE stated that localized corrosion could occur if the corrosion potential,  $E_{corr}$ , exceeded a critical potential, which DOE defined as the repassivation potential,  $E_{rcrev}$ . The corrosion potential is a function of the chemical environment, kinetic rates controlling the speed or rate of corrosion, and the temperature. The repassivation potential is a property of the material, but it can also be affected by chemical conditions and temperature. Based on electrochemical tests under a range of chemical environments, DOE derived (via curve fitting) the following empirical equations to compute the repassivation and the corrosion potentials:

$$E_{rcrev} = a_0 + a_1 T + a_2 \ln[Cl^-] + a_3 \frac{[NO_3^-]}{[Cl^-]} + a_4 T [Cl^-] + \epsilon_{rcrev} \quad (3-1)$$

and

$$E_{corr} = c_0 + c_1 T + c_2 pH + c_3 \frac{[NO_3^-]}{[Cl^-]} + c_4 T \frac{[NO_3^-]}{[Cl^-]} + c_5 pH \frac{[NO_3^-]}{[Cl^-]} + c_6 pH \ln[Cl^-] + \epsilon_{corr} \quad (3-2)$$

where

—  $E_{rcrev}$  and  $E_{corr}$  are potentials in units of mV versus saturated calomel electrode [mV<sub>SCE</sub>]

—  $a_0$  through  $a_4$  and  $c_0$  through  $c_6$  are fitting constants (see Tables 3-1 and 3-2)

—  $T$  is the temperature in Celsius units

Table 3-1. Mean, Standard Deviation, and Covariance Matrix for the Parameters $a_0$ Through $a_4$ *					
	$a_0$	$a_1$	$a_2$	$a_3$	$a_4$
Mean	190.242	-3.008	-46.8	535.625	0.061
Sdev	18.373	0.225	3.126	26.14	0.01
Covariance Matrix					
	$a_0$	$a_1$	$a_2$	$a_3$	$a_4$
$a_0$	337.6	-3.909	-9.31	82.36	0.03559
$a_1$	-3.909	0.05077	0.09271	-1.202	-0.000831
$a_2$	-9.31	0.09271	9.77	1.93	-0.02048
$a_3$	82.36	-1.202	1.93	683.3	-0.0279
$a_4$	0.03559	-0.000831	-0.02048	-0.0279	0.0001011
*SNL. "General Corrosion and Localized Corrosion of Waste Package Outer Barrier." ANL-EBS-MD-000003. Rev. 03. ACN 01, ERD 01. Las Vegas, Nevada: Sandia National Laboratories. 2007.					

<b>Table 3-2. Mean, Standard Deviation, and Covariance Matrix for the Parameters <math>c_0</math> Through <math>c_6</math>*</b>							
	$c_0$	$c_1$	$c_2$	$c_3$	$c_4$	$c_5$	$c_6$
Mean	1051.219	-3.024	-155.976	-1352.04	10.875	137.856	-8.498
Sdev	119.774	0.977	11.495	252.224	1.89	23.158	0.801
<b>Covariance Matrix</b>							
	$c_0$	$c_1$	$c_2$	$c_3$	$c_4$	$c_5$	$c_6$
$c_0$	14350	-103.1	-915.2	-27620	180.2	1884	-16.6
$c_1$	-103.1	0.9539	2.77	184.6	-1.519	-6.817	-0.07543
$c_2$	-915.2	2.77	132.1	1971	-6.909	-251.5	4.409
$c_3$	-27620	184.6	1971	63620	-422.3	-4107	59.59
$c_4$	180.2	-1.519	-6.909	-422.3	3.573	13.37	-0.2622
$c_5$	1884	-6.817	-251.5	-4107	13.37	536.3	-6.697
$c_6$	-16.6	-0.07543	4.409	59.59	-0.2622	-6.697	0.6418
*SNL. "General Corrosion and Localized Corrosion of Waste Package Outer Barrier." ANL-EBS-MD-000003. Rev. 03. ACN 01, ERD 01. Las Vegas, Nevada: Sandia National Laboratories. 2007.							

—  $[Cl^-]$  is the chloride ion concentration in molal units [mol/kg H<sub>2</sub>O]

—  $[NO_3^-]$  is the nitrate ion concentration in molal units [mol/kg H<sub>2</sub>O]

—  $\epsilon_{rcrev}$  and  $\epsilon_{corr}$  are terms to correct for fitting errors

DOE accounted for fitting uncertainty by describing the parameters  $a_1$  through  $c_6$  as correlated random variates following normal distributions. The parameters of those distributions are provided in Tables 3-1 and 3-2. The error terms  $\epsilon_{rcrev}$  and  $\epsilon_{corr}$  are terms independent of the fitting parameters, assumed to follow normal distributions with zero means and standard deviations equal to 45.055 mV and 85.265 mV, respectively.

In the performance assessment analysis, to account for fitting uncertainty, DOE sampled 5-tuples ( $a_0, a_1, a_2, a_3, a_4$ ) and 7-tuples ( $c_0, c_1, c_2, c_3, c_4, c_5, c_6$ ) from multinormal distributions with means, standard deviations, and covariance matrices as in Tables 3-1 and 3-2, and used those N-tuples to compute  $E_{rcrev}$  and  $E_{corr}$  using Eqs. (3-1) and (3-2) in multiple-realization analyses. DOE considered the standard deviations in the error terms  $\epsilon_{rcrev}$  and  $\epsilon_{corr}$

(45.055 mV and 85.265 mV) to define truncation boundaries ( $\pm 2$  standard deviations around expected values of  $E_{rcrev}$  and  $E_{corr}$ ) for the repassivation and corrosion potentials. DOE imposed the  $\pm 2$  standard deviations bounds to avoid nonphysical situations that could arise due to the mathematical sampling algorithms. More explicitly, the corrosion and repassivation potentials were computed as

$$E_{rcrev} = \mathbf{A} \cdot \mathbf{E}_a \quad (3-3)$$

and

$$E_{corr} = \mathbf{C} \cdot \mathbf{E}_c \quad (3-4)$$

where the operator “ $\cdot$ ” is a scalar dot product and the vectors  $\mathbf{A}$ ,  $\mathbf{E}_a$ ,  $\mathbf{C}$ , and  $\mathbf{E}_c$  are defined as

$$\mathbf{A} = (a_0 \quad a_1 \quad a_2 \quad a_3 \quad a_4) \quad (3-5)$$

$$\mathbf{E}_a = \left( 1 \quad T \quad \ln[Cl^-] \quad \frac{[NO_3^-]}{[Cl^-]} \quad T[Cl^-] \right) \quad (3-6)$$

$$\mathbf{C} = (c_0 \quad c_1 \quad c_2 \quad c_3 \quad c_4 \quad c_5 \quad c_6) \quad (3-7)$$

$$\mathbf{E}_c = \left( 1 \quad T \quad pH \quad \frac{[NO_3^-]}{[Cl^-]} \quad T \frac{[NO_3^-]}{[Cl^-]} \quad pH \frac{[NO_3^-]}{[Cl^-]} \quad pH \ln[Cl^-] \right) \quad (3-8)$$

The vectors  $\mathbf{A}$  and  $\mathbf{C}$  are tuples obtained by randomly sampling multinormal distributions with means and covariance matrices as in Tables 3-1 and 3-2. If  $\mathbf{A}_m$  and  $\mathbf{C}_m$  are the tuples with the mean values (second row in Tables 3-1 and 3-2), and  $\mathbf{M}_a$  and  $\mathbf{M}_c$  are covariance matrices in Tables 3-1 and 3-2, bounds for the repassivation and corrosion potential were defined by the following inequalities

$$\|E_{rev} - \mathbf{A}_m \cdot \mathbf{E}_a\| \leq 2\sqrt{\mathbf{E}_a \mathbf{M}_a \mathbf{E}_a^T + 45.055^2} \quad (3-9)$$

and

$$\|E_{corr} - \mathbf{C}_m \cdot \mathbf{E}_c\| \leq 2\sqrt{\mathbf{E}_c \mathbf{M}_c \mathbf{E}_c^T + 85.265^2} \quad (3-10)$$

For those values of  $\mathbf{A}$  and  $\mathbf{C}$  for which the previous inequalities were not satisfied, the repassivation and the corrosion potentials were computed as

$$E_{rev} = \mathbf{A}_m \cdot \mathbf{E}_a \pm 2\sqrt{\mathbf{E}_a \mathbf{M}_a \mathbf{E}_a^T + 45.055^2} \quad (3-11)$$

and

$$E_{corr} = \mathbf{C}_m \cdot \mathbf{E}_c \pm 2\sqrt{\mathbf{E}_c \mathbf{M}_c \mathbf{E}_c^T + 85.265^2} \quad (3-12)$$

The selection of the + or – signs in the previous equations depends on whether the computed value of the potential computed from Eqs. (3-3) and (3-4) lies too far above or below the expected values,  $\mathbf{A}_m \cdot \mathbf{E}_a$  or  $\mathbf{C}_m \cdot \mathbf{E}_c$ .

This detailed description of the approach adopted to compute the repassivation and corrosion potential is provided because it is very common to make the mistake of only analyzing the equations with the best fit parameters (mean row in Tables 3-1 and 3-2) and ignoring standard deviations and covariance matrices. As described in the previous paragraphs, DOE implemented a more complex algorithm to propagate fitting uncertainty.

DOE defined the repassivation and corrosion potentials as functions of the similar independent variables. This causes  $E_{rev}$  and  $E_{corr}$  to be heavily correlated. For example, using the best fit

values for the parameters  $a_0$  through  $c_6$  (mean rows in Tables 3-1 and 3-2) and Eqs. (3-1) and (3-2),  $E_{rcrev}$  can be defined as a function of  $E_{corr}$ ,  $T$ ,  $pH$ , and  $[Cl^-]$  as

$$E_{rcrev} = 190.242 - 3.008 T + 0.061 T [Cl^-] - 46.8 \ln[Cl^-] + \frac{563059 - 535.625 E_{corr} - 83544.6 pH - 1619.73 T - 4551.74 pH \ln[Cl^-]}{1352.04 - 137.856 pH - 10.875 T} \quad (3-13)$$

$E_{rcrev}$  and  $E_{corr}$  are linearly related, and this is true for any selection of values of the fitting parameters  $a_0$  through  $c_6$ . Whether the  $E_{rcrev}$  increases or decreases with increasing values of  $E_{corr}$  depends on whether the denominator on the second term in Eq. (3-13) is negative or positive. Given the strong correlation between these electric potentials, analyses of Eqs. (3-1) and (3-2) aimed at independently delineating the environmental conditions that cause  $E_{rcrev}$  or  $E_{corr}$  to attain high or low values do not provide a complete picture of conditions conducive to localized corrosion. In the analysis presented in this report, both equations are simultaneously considered for particular water chemistries and temperatures to establish whether localized corrosion could occur under those conditions.

Several approaches were considered to establish ranges of chemical conditions and temperatures that could lead to localized corrosion of Alloy 22. For example, equations similar to Eq. (3-13) were derived and trends and slopes with respect to the independent variables were analyzed. Also, the limits defined by Eqs. (3-11) and (3-12) were examined. The objective was to derive ranges of environmental conditions under which  $E_{corr} > E_{rcrev}$ . Those approaches were cumbersome and lacked generality, as they were dependent on values assigned to the fitting parameters  $a_0$  through  $a_6$ . Therefore, those approaches are not further discussed. In this report, general conclusions were attained by fixing the environmental conditions {e.g.,  $T = 90^\circ C$ ,  $[194^\circ F]$ ,  $[NO_3^-]/[Cl^-] = 0.2$ ,  $[Cl^-] = 1$  molal,  $pH = 8$ } and quantifying the probability that  $E_{corr} > E_{rcrev}$  for those particular conditions. The probability that  $E_{corr} > E_{rcrev}$  for a particular water chemistry and temperature {e.g.,  $T = 90^\circ C$   $[194^\circ F]$ ,  $[NO_3^-]/[Cl^-] = 0.2$ ,  $[Cl^-] = 1$  molal,  $pH = 8$ } was quantified by a Monte Carlo analysis. In each realization, a 5-tuple ( $a_0, a_1, a_2, a_3, a_4$ ) and a 7-tuple ( $c_0, c_1, c_2, c_3, c_4, c_5, c_6$ ) were sampled from multinormal distributions with means, standard deviations, and covariance matrices as in Tables 3-1 and 3-2 (multinormal sampling functions are available in scientific software such as Mathematica®). With those N-tuples, the repassivation and corrosion potentials were computed. A total of 10,000 realizations were implemented for each environmental condition. The probability for localized corrosion was quantified as the number of realizations for which  $E_{corr} > E_{rcrev}$  normalized by the total number of realizations (i.e., 10,000). Figure 3-1 shows a schematic plot that corresponds to this approach. The probability  $P(E_{corr} > E_{rcrev})$  is computed as a function of  $pH$  for a fixed value of  $T$ ,  $[NO_3^-]/[Cl^-]$ , and  $[Cl^-]$  and results in a curve as in Figure 3-1. When the  $pH$  is low enough, it is more likely that  $E_{corr} > E_{rcrev}$ . As the  $pH$  increases, the probability decreases and it eventually becomes negligible.

Figure 3-2 shows families of curves for temperatures ranging from 20 to 110 °C [68 to 230 °F],  $[Cl^-]$  from 0.0005 to 20 molal,  $[NO_3^-]/[Cl^-]$  from 0 to 10, and  $pH$  from 1.9 to 10. Only discrete values in those ranges were selected; however, the discrete values allow for general conclusions by interpolation of the trends. All the curve families exhibit a similar shape as Figure 3-1. The exception is curves for low  $[Cl^-]$  and high  $[NO_3^-]/[Cl^-]$  ratios, which appear to imply that at low chloride concentrations, the probability of localized corrosion increases with increasing  $pH$ . The meaning of the trends is discussed later in this report.

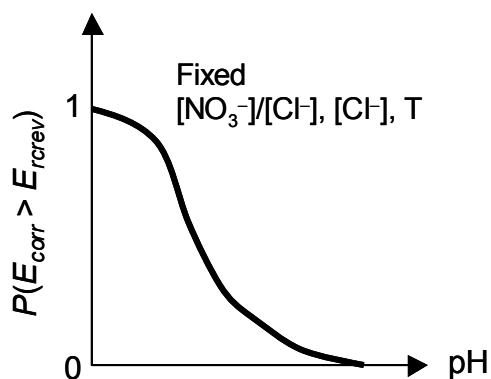


**Figure 3-1. Schematic of Curve Derived With the Monte Carlo Approach To Quantify  $P(E_{corr} > E_{rev})$**

The different colors represent variation in temperature from 20 °C [68 °F] (blue) to 110 °C [230 °F] (red) in discrete increments of 10 °C [18 °F]. As temperature increases, the probability versus pH curves shift to the right. In other words, as the temperature decreases, lower pH solutions are needed to induce localized corrosion. This trend is consistent with empirical knowledge. The trend changes in the limit of low nitrate-to-chloride ratio and high chloride [see Figure 3-2(c)]. When the chloride concentration is high (~10 molal) and the nitrate concentration is negligible, the pH of solutions causing localized corrosion decreases with increasing temperature. The other exception to the general trend occurs in the limit of high nitrate-to-chloride ratio (>0.5) and low chloride concentration [e.g., Figure 3-2(m), (p), (t)]. This exception is discussed later in this report. In general, for most of the solutions of interest, as the temperature decreases, localized corrosion requires more acidic or lower pH solutions.

The effect of increasing ratio in nitrate to chloride can be seen by sweeping the plots across a column, from the top down. As the ratio increases, in general, the plots are shifted toward the left, meaning that solutions of lower pH are needed to induce localized corrosion as  $[NO_3^-]/[Cl^-]$  increases. This trend is intuitive because  $[NO_3^-]$  is a known localized corrosion inhibitor in Alloy 22. This trend is broken at high  $[NO_3^-]/[Cl^-]$  and low  $[Cl^-]$  [e.g., Figure 3-2(m), (p), (t)]. In low  $[Cl^-]$  solutions, it appears that adding  $[NO_3^-]$  to the solution would enhance the likelihood of localized corrosion at high enough temperatures. It is hypothesized that this is mostly a mathematical artifact, because such low  $[Cl^-]$  environments are not likely to exist at elevated temperatures. For example, in Figure 2-6,  $[Cl^-]$  exceeds 1 molal for all temperatures above 50 °C [122 °F]. Low chloride concentrations were computed only at the ambient temperature. Therefore, the curves with  $T > 50$  °C [122 °F] in Figure 3-2(m), (p), (t) represent nonphysical conditions {not possible to have a solution in thermodynamic equilibrium with  $[Cl^-] = 0.0005$  molal at those temperatures, under the pressure and partial water pressure conditions defined in Chapter 2}. The low temperature curves {e.g.,  $T = 20$  °C [68 °F]} for which  $[Cl^-] = 0.0005$  molal is feasible lie on the pH axis and cannot be seen, because they are overlapped by the higher temperature curves in Figure 3-2(m), (p), (t). The curves  $T = 20$  °C [68 °F],  $[Cl^-] = 0.0005$  molal, and  $[NO_3^-]/[Cl^-] > 0.5$  support the empirical notion that localized corrosion is unlikely under such conditions.

In Figure 3-2, the effect of increasing chloride concentration can be visualized by scanning the plots from left to right, across a row. Increasing chloride has the effect of shifting probability versus pH curves toward the left. It means that lower pH solutions are needed to cause localized corrosion in Alloy 22 in solutions with high chloride concentration. This trend is counterintuitive. The exception to this general behavior is the case of low chloride and high

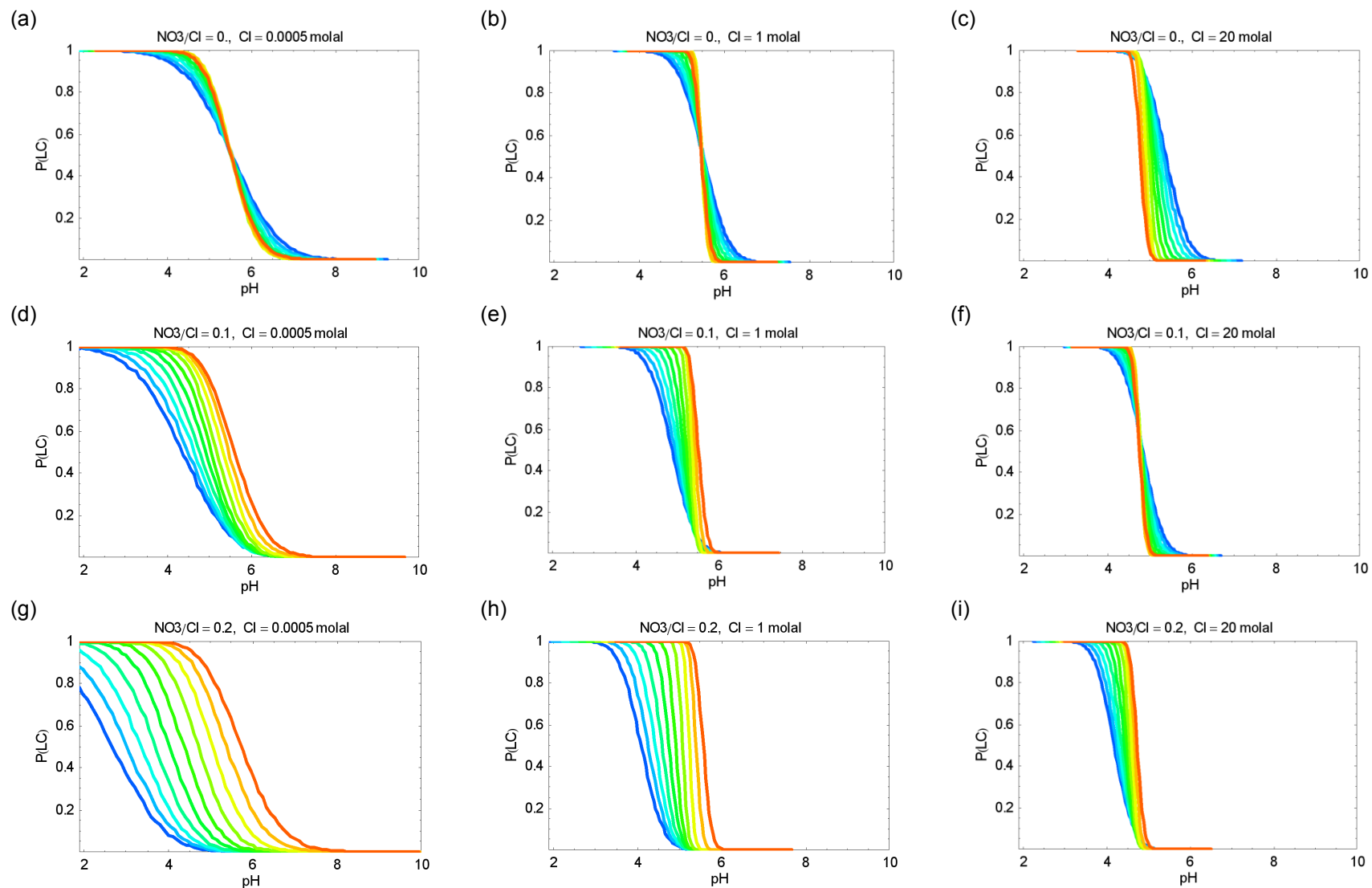


**Figure 3-2. Probability of  $E_{corr} > E_{rev}$  as a Function of pH, Chloride, and Nitrate Concentration and Temperature**

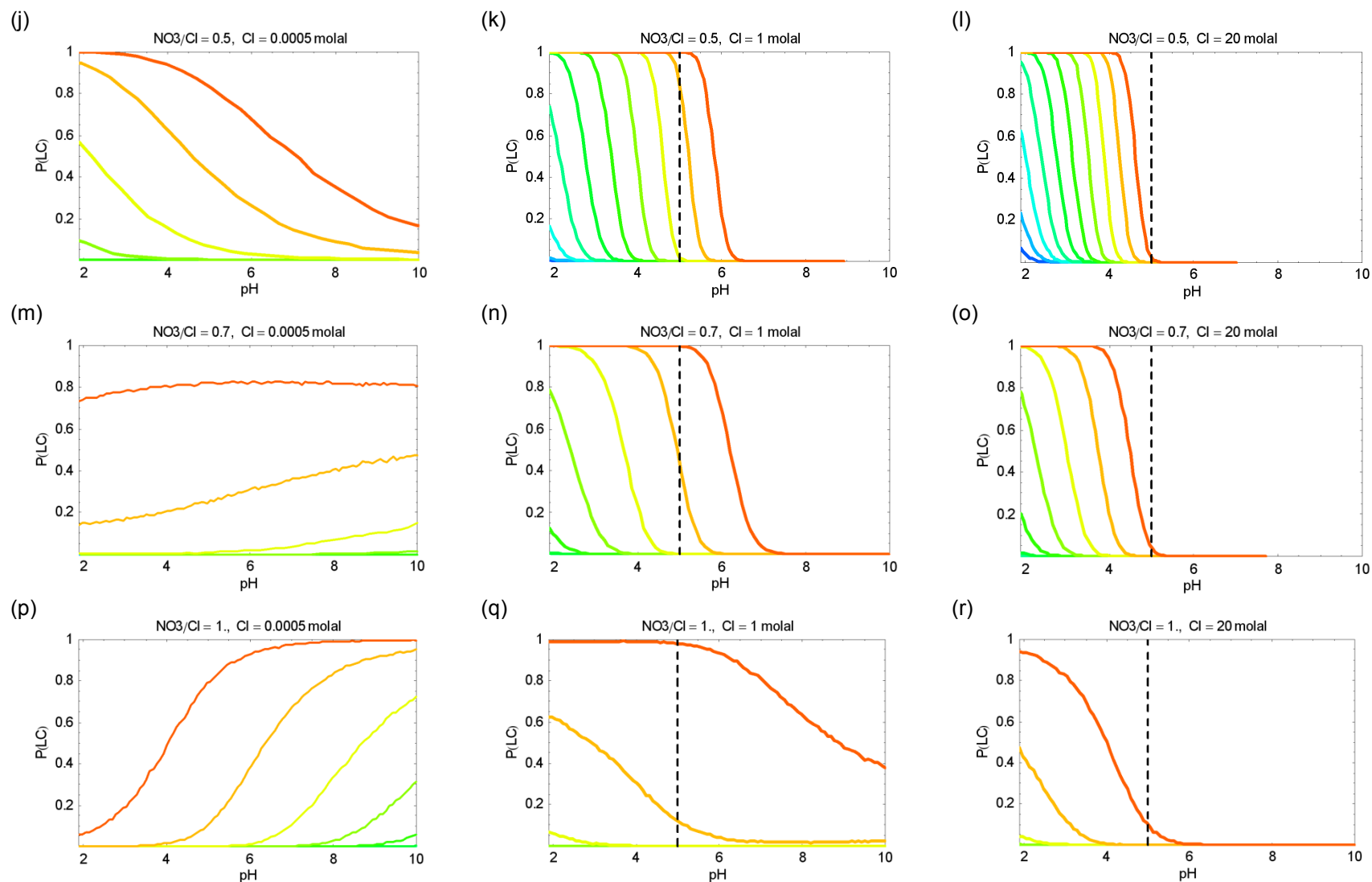


**Figure 3-2. Probability of  $E_{corr} > E_{rev}$  as a Function of pH, Chloride, and Nitrate Concentration, and Temperature (continued)**



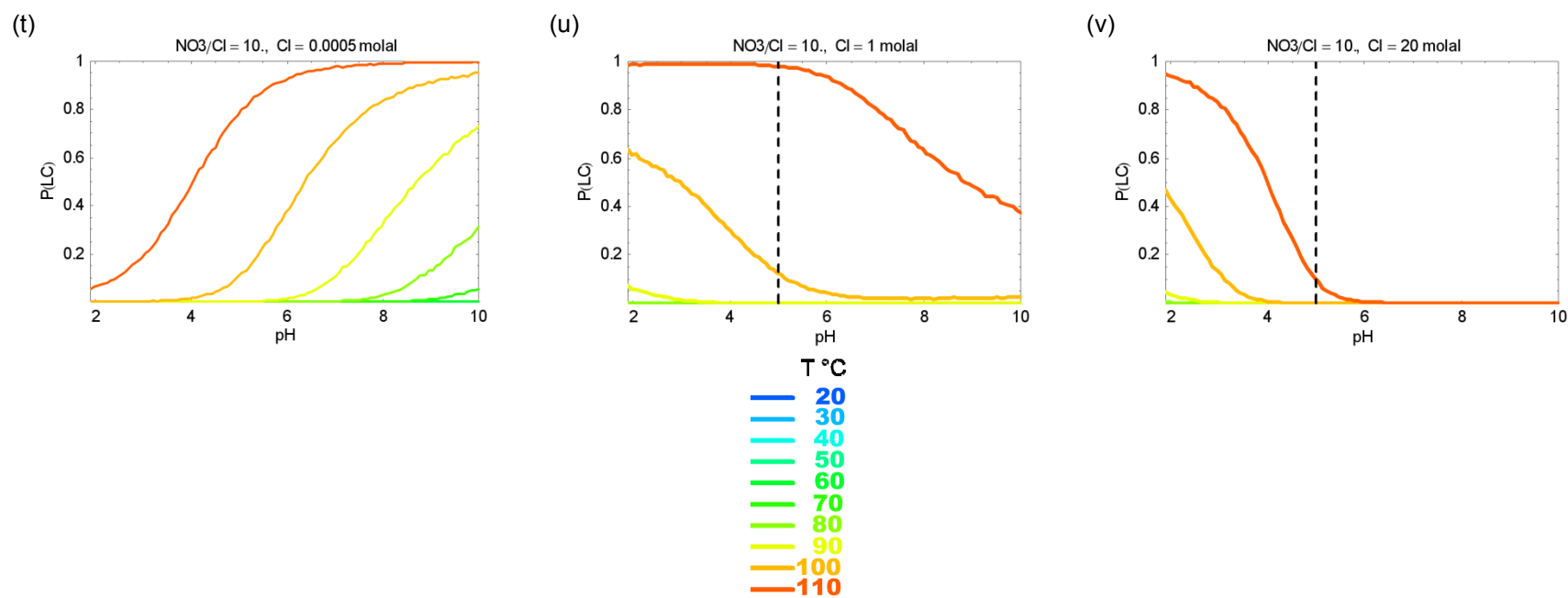


Figure 3-2. Probability of  $E_{corr} > E_{rcrev}$  as a Function of pH, Chloride, and Nitrate Concentration, and Temperature (continued)

nitrate-to-chloride ratios [Figure 3-2(m), (p), (t)], which was analyzed in the previous paragraph and not discussed further. There is a physical basis for the nonintuitive behavior. As chloride is added to the system, it displaces oxygen from the solution causing the corrosion potential to decrease. The coefficient  $c_6$  in Eq. (3-2) is negative, which means that for constant values of  $T$ ,  $pH$ , and  $[NO_3^-]/[Cl^-]$ ,  $E_{corr}$  is a decreasing function of  $[Cl^-]$ . Most likely, as previously stated, the cause for this decreasing trend is this displacement of oxygen and other oxidants in the solution by increasing chloride concentrations.  $E_{rcrev}$  is also expected to be a decreasing function of  $[Cl^-]$ ; however,  $E_{corr}$  decreases faster than  $E_{rcrev}$  with increasing  $[Cl^-]$ . The final outcome of those competing trends is the nonintuitive result that more acidic solutions are needed to induce localized corrosion in solutions with increasing  $[Cl^-]$ . Although nonintuitive, the empirical data from which Eqs. (3-1) and (3-2) were derived support this conclusion (DOE, 2009b, Enclosure 8).

This chapter concludes with a summary of conditions under which, according to Eqs. (3-1) and (3-2), the values in Tables 3-1 and 3-2, and the thermodynamic analyses in Chapter 2, localized corrosion could occur. For  $[NO_3^-]/[Cl^-] \geq 0.5$ , localized corrosion could occur at  $T > 80^\circ C$  [ $176^\circ F$ ]. Note that in Figure 3-2(k), (l), (n), (o), (q), (r), (u), (v), the vertical dotted line is drawn at  $pH = 5$ . The  $pH$ s of most solutions considered in Chapter 2 for the median relative humidity case are greater than 5 (Figures 2-6 and 2-13). All of the curves for  $T \leq 80^\circ C$  [ $176^\circ F$ ] lie to the left of the line  $pH = 5$ . Therefore, none of the solutions considered in Chapter 2 with  $T \leq 80^\circ C$  [ $176^\circ F$ ] and  $[NO_3^-]/[Cl^-] \geq 0.5$  can cause localized corrosion. Localized corrosion, on the other hand, might be feasible for  $T > 80^\circ C$  [ $176^\circ F$ ], even at those high  $[NO_3^-]/[Cl^-]$  ratios.

For lower  $[NO_3^-]/[Cl^-]$  ratios ( $<0.5$ ), 0.001 probability boundaries were computed with the data in Figure 3-2 for discrete values of  $[Cl^-]$  (0.0005, 0.01, 0.1, 1, and 20 molal). For a particular set of conditions  $\{T, [NO_3^-]/[Cl^-], \text{ and } [Cl^-]\}$ , the  $pH$  at which  $P(E_{corr} > E_{rcrev}) = 0.001$  was computed by interpolation of the probability versus  $pH$  curves. These computation results are presented in Figure 3-3, where the dotted lines represent the ranges of  $pH$  computed in Figure 2-2 for the various temperatures. The curves of different colors represent the various chloride concentrations. The curves can be interpreted as localized corrosion boundaries. In solutions with a  $pH$  that lies above the curves, localized corrosion is unlikely to happen (the probability is at most 0.001). The curves also show the nonintuitive behavior previously discussed: as  $[Cl^-]$  increases, a solution of lower  $pH$  is needed for localized corrosion to occur. As nitrate is added to the system, the boundary curves are displaced downwards in the low  $T$  range. This means that if nitrate is present in the system, solutions with lower  $pH$  are needed to induce localized corrosion at lower temperatures. At higher temperatures, adding  $[NO_3^-]$  appears to enhance the susceptibility for localized corrosion, especially when  $[Cl^-]$  is low (e.g., less than 0.1 molal). However, for the pressure and water pressure conditions considered in Chapter 2, solutions of that low  $[Cl^-]$  do not appear to be under thermodynamic equilibrium and would evolve toward solutions of higher  $[Cl^-]$ . All of the thermodynamic equilibrium solutions considered in Chapter 2 resulted in  $[Cl^-]$  exceeding 1 molal for  $T \geq 50^\circ C$  [ $122^\circ F$ ]. The  $[Cl^-] = 1$  molal curve boundary in Figure 3-3 is the yellow line (second line from the bottom). All of the solution  $pH$ s from

Figure 2-2 (range represented by the dotted lines) lie above the yellow line, except at  $T = 110^\circ C$  [ $230^\circ F$ ]. Therefore, it is concluded that localized corrosion for  $T \leq 90^\circ C$  [ $194^\circ F$ ] is unlikely for  $[NO_3^-]/[Cl^-] < 0.5$  on the basis that the needed low  $pH$  solutions are unlikely to arise. There is one exception to this statement. In Figure 3-3(a), the dotted line for  $pH$  at  $T = 25^\circ C$  [ $77^\circ F$ ] crosses the blue line  $[Cl^-] = 0.0005$  molal. This means that, according to Eqs. (3-1) and

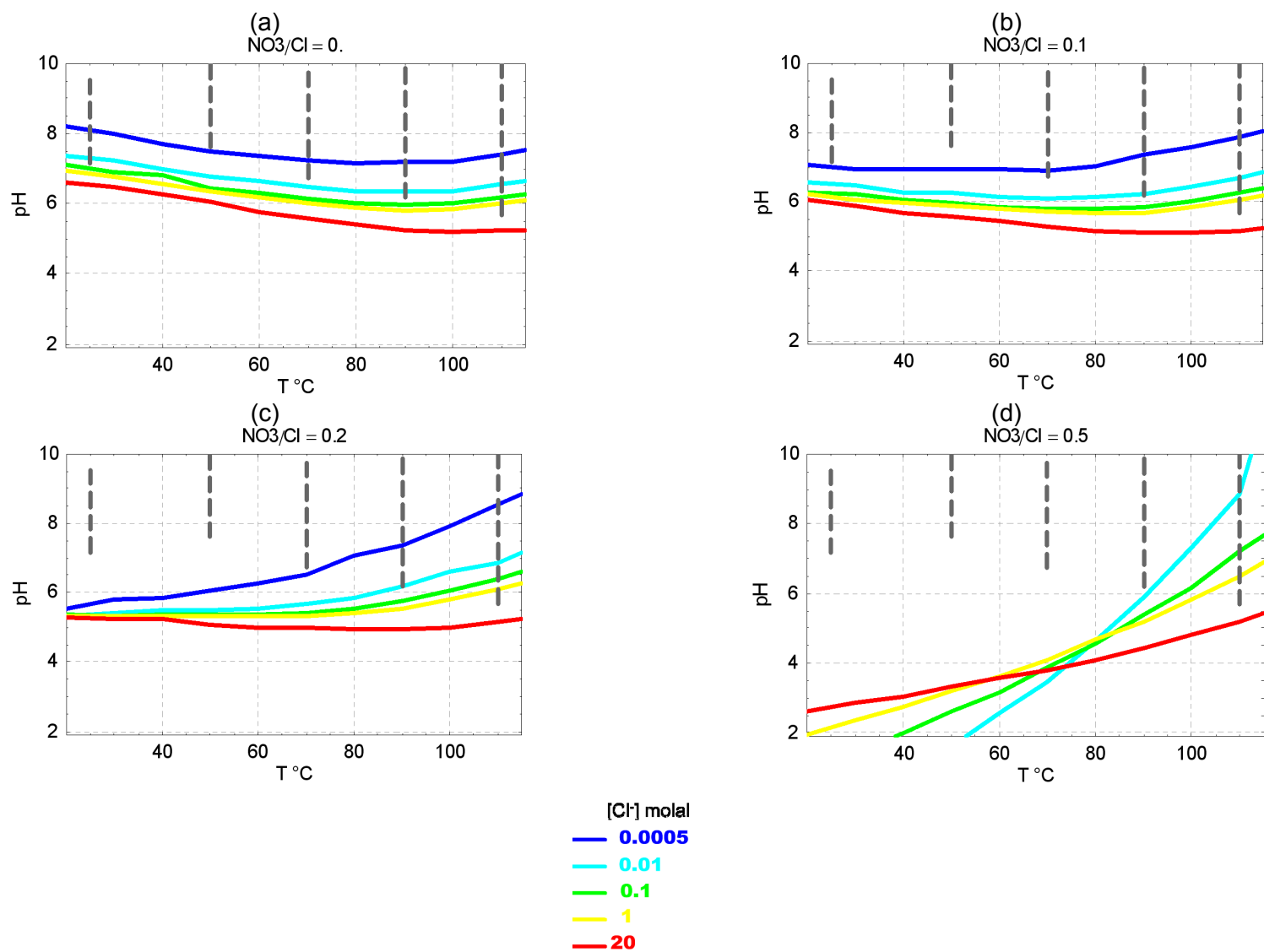


**Figure 3-3. Localized Corrosion Boundaries (Probability = 0.001) as a Function of Chloride and Nitrate Concentrations and Temperature. The Dotted Lines Represent the pH Ranges in Figure 2-2.**

(3-2), localized corrosion is likely at low  $T$ , provided there is negligible  $[\text{NO}_3^-]$  in the solution. A minor amount of nitrate, however, would render localized corrosion unlikely [see Figure 3-3(b)]. This prediction of the possibility of localized corrosion at low temperatures if the nitrate concentration is negligible is only a mathematical artifact of the curve fitting. Localized corrosion in Alloy 22 has not been observed under such environmental conditions.

In conclusion, localized corrosion only appears likely (probability  $>0.001$ ) at  $T > 80^\circ\text{C}$  [ $176^\circ\text{F}$ ]. The solutions in Chapter 2 have a pH sufficiently high that it is unlikely (probability  $<0.001$ ) for Alloy 22 localized corrosion to occur (i.e.,  $E_{\text{corr}} > E_{\text{rev}}$ ) for all solutions with  $T \leq 80^\circ\text{C}$

[ $176^\circ\text{F}$ ]. Figure 3-4 is a range of temperatures at the waste package surface from DOE [2008, Figure 2.3.5-33(b)]. According to such range of temperatures, the waste package is estimated to be below  $80^\circ\text{C}$  [ $176^\circ\text{F}$ ] after 3,500 years or sooner. Beyond 12,000 years, the waste package temperature is expected to drop below  $50^\circ\text{C}$  [ $122^\circ\text{F}$ ]. From Figure 3-3, when  $T < 50^\circ\text{C}$  [ $122^\circ\text{F}$ ] and with a marginal amount of nitrate, the needed pH to cause localized corrosion is too low and unlikely to arise. DOE reported the computation of localized corrosion conditions extending up to around 12,000 years (DOE, 2009a, Enclosure 1). Such results are reproduced in Figure 3-5. From this figure, note that beyond 3,500 years, the probability for Alloy 22 localized corrosion drops below 0.001, which is consistent with results in this report. Beyond 3,500 years, DOE computed that localized corrosion could occur mainly in midpercolation range regions (DOE divided the repository into 5 percolation bins). This DOE result is consistent with the analysis in this report. For low percolation rate regions or bins, the

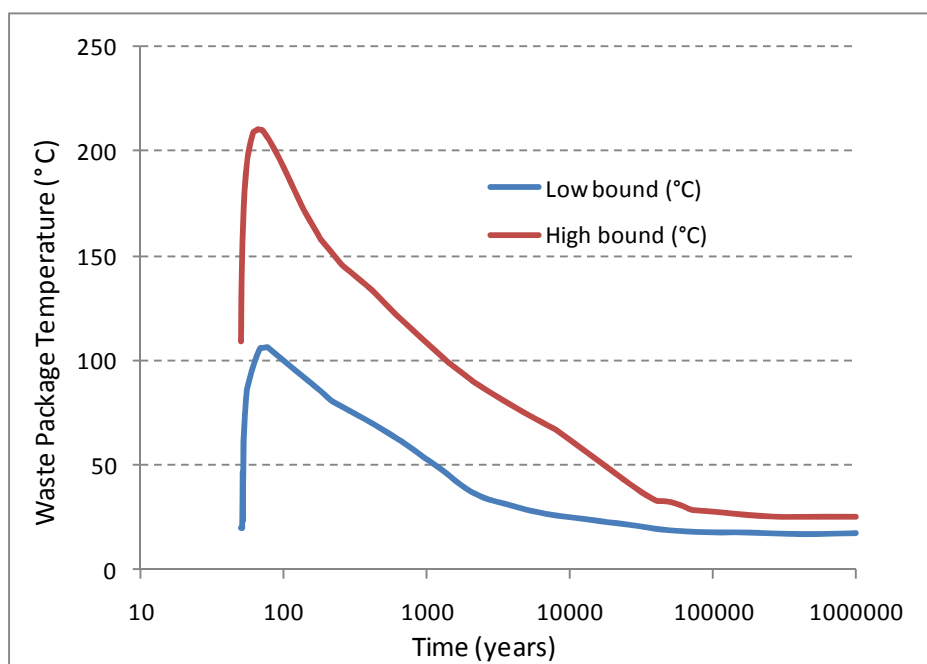


**Figure 3-4. Range of Waste Package Temperatures Reproduced From DOE [2008, Figure 2.3.5-33(b)]**

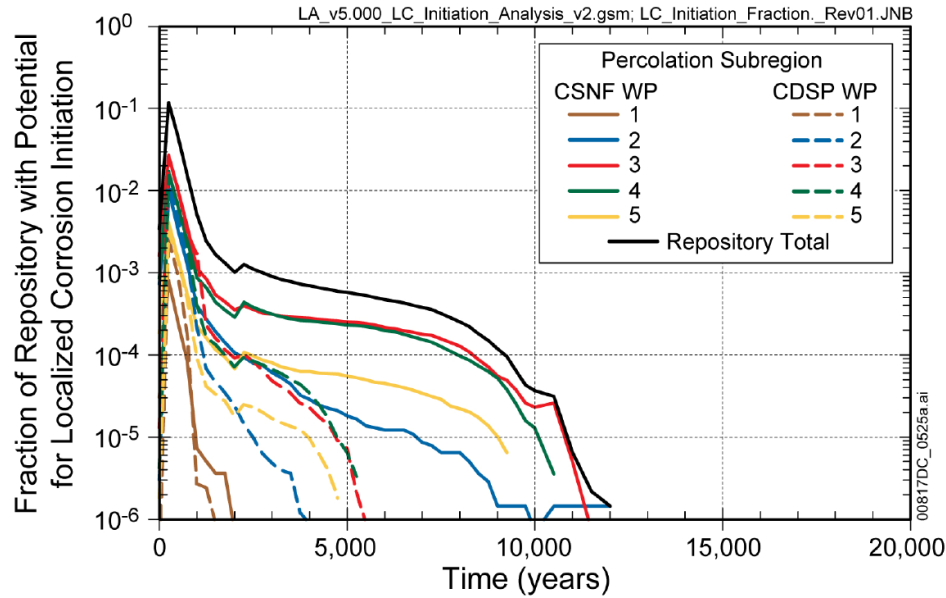


**Figure 3-5. DOE Computation of the Probability of Localized Corrosion as a Function of the Drip Shield Failure Time. Source: DOE (2009a, Enclosure 1, Figure 2).**

temperature tends to be higher and the system drier, causing chloride concentrations to be higher and localized corrosion less likely. For the high percolation rate region, the temperature is lower, the relative humidity is higher, and the range of pH tends to be higher, making localized corrosion less likely. In the midrange of the percolation—where the temperatures and relative humidities are relatively high to cause the formation of low pH solutions and low chloride concentrations—the DOE equations predict a higher chance for localized corrosion provided there is no nitrate in the solution [see Figures 3-3(a) and 3-5]. Note, however, that localized corrosion of Alloy 22 has never been detected in low temperature solutions with low chloride concentrations. Such computation of localized corrosion is most likely an artifact of the mathematical curve fitting.

## 4 SUMMARY AND CONCLUSIONS

Seepage water evaporation could lead to the formation of corrosive brines on waste package surfaces and promote localized corrosion. The potential brine chemistry is a function of the initial water composition (i.e., composition of seepage water), air pressure and water content in air (i.e., relative humidity), and the temperature of the EBS materials that the solutions are postulated to contact. In this study, thermodynamic simulations of seepage water evaporation were conducted to determine the potential chemistry of these brines. The likelihood that these brines would be capable of supporting initiation and propagation of localized corrosion of the Alloy 22 waste package material was analyzed. The results indicate that Alloy 22 localized corrosion is likely (probability  $>0.001$ ) only at  $T > 80\text{ }^{\circ}\text{C}$  [ $>176\text{ }^{\circ}\text{F}$ ]. At  $T \leq 80\text{ }^{\circ}\text{C}$  [ $\leq 176\text{ }^{\circ}\text{F}$ ], the brines would have a sufficiently high pH such that localized corrosion would be unlikely (probability  $<0.001$ ). The analysis also indicates that when  $T < 50\text{ }^{\circ}\text{C}$  [ $<122\text{ }^{\circ}\text{F}$ ] and a marginal amount of nitrate is present in solution, the solution pH is unlikely to be low enough to cause localized corrosion.

The DOE localized corrosion model implies that increasing chloride concentrations could reduce the potential for Alloy 22 localized corrosion. It was hypothesized that an increasing concentration of chloride displaces oxygen and other oxidants in the solution, causing the corrosion potential to decrease. On the other hand, increasing chloride concentration causes the repassivation potential to decrease. The net effect of these competing trends is the nonintuitive result (noted in the computations in this report) that localized corrosion is less likely in solutions of increasing chloride concentration. This nonintuitive trend was used to rationalize DOE results that showed varying probability for localized corrosion as a function of deep percolation rates. For the low percolation rate region, the temperature tends to be higher and the system drier, causing chloride concentrations to be higher and localized corrosion to be less likely. For the high percolation rate region, the temperature is lower, the relative humidity higher, and the range of pH tends to be higher, which makes localized corrosion less likely. In the midrange of the percolation rates—where the temperature and relative humidity are comparatively high, causing solutions with low pH and low chloride concentration to form—localized corrosion has a slightly higher chance of occurrence. The independent computations based on the DOE model predict that localized corrosion would occur in solutions of low chloride concentration and low temperature; however, it is argued that this prediction is most likely an artifact of the mathematical curve fitting, because localized corrosion of Alloy 22 has never been detected in this type of environment.

## 5 REFERENCES

Browning, L., W.M. Murphy, B.W. Leslie, and W.L. Dam. "Thermodynamic Interpretations of Chemical Analyses of Unsaturated Zone Water from Yucca Mountain, Nevada." Symposium on the Scientific Basis for Nuclear Waste Management XXIII. R. Smith and D. Shoesmith, eds. Materials Research Society Symposium Proceedings. Vol. 608. Warrendale, Pennsylvania: Materials Research Society. pp. 237–242. 2000.

DOE. "Yucca Mountain—Response to Request for Additional Information Regarding License Application (Safety Analysis Report Section 2.3.6.8), Safety Evaluation Report Vol. 3, Chapter 2.2.1.3.1, Set 2." Letter (April 8) to J.H. Sulima (NRC) from J.R. Williams. ML090980537. Washington, DC: DOE, Office of Technical Management. 2009a.

\_\_\_\_\_. "Yucca Mountain—Response to Request for Additional Information Regarding License Application (Safety Analysis Report Section 2.3.6.8), Safety Evaluation Report Vol. 3, Chapter 2.2.1.3.1, Set 2." Letter (April 13) to J.H. Sulima (NRC) from J.R. Williams. ML091100634. Washington, DC: DOE, Office of Technical Management. 2009b.

\_\_\_\_\_. DOE/RW-0573, "Yucca Mountain Repository License Application." Rev. 0. ML081560400. Las Vegas, Nevada: DOE, Office of Civilian Radioactive Waste Management. 2008.

Gerbino, A. "A Guide for Using the OLI Analyzers." Morris Plains, New Jersey: OLI Systems, Inc. 2006.

Gruszkiewicz, M.S., D.A. Palmer, R.D. Springer, P. Wang, and A. Anderko. "Phase Behavior of Aqueous Na–K–Mg–Ca–Cl–NO<sub>3</sub> Mixtures: Isopiestic Measurements and Thermodynamic Modeling." *Journal of Solution Chemistry*. Vol. 36. pp. 723–765. 2007.

Hardie, L.A. and H.P. Eugster. "The Revolution of Closed-Basin Brines." *Mineralogical Society of America Special Paper*. Vol. 3. pp. 273–290. 1970.

Harrar, J.E., J.F. Carley, W.F. Isherwood, and E. Raber. "Report of the Committee To Review the Use of J-13 Well Water in Nevada Nuclear Waste Storage Investigations." UCID-21867. Livermore, California: Lawrence Livermore National Laboratory. 1990.

Leslie, B., C. Grossman, and J. Durham. "Total-System Performance Assessment (TPA) Version 5.1 Module Descriptions and User Guide." Rev. 1. San Antonio, Texas: Center for Nuclear Waste Regulatory Analyses. 2007.

Manepally, C. and R. Fedors. "Edge-Cooling Effect on the Potential Thermohydrologic Conditions at Yucca Mountain." Proceedings of the 10<sup>th</sup> International High-Level Radioactive Waste Management Conference, Las Vegas, Nevada, March 30–April 3, 2003. La Grange Park, Illinois: American Nuclear Society. Published in CD-ROM. 2003.

OLI Systems, Inc. "A Guide to Using OLI Analyzer Studio Version 3.1." Morris Plains, New Jersey: OLI Systems, Inc. 2010.

Pensado, O. and R. Pabalan. "Probabilistic Methodology To Estimate Environmental Conditions for Localized Corrosion and Stress Corrosion Cracking of Alloy 22 in a High Level Radioactive Waste Repository Setting." *Journal of Nuclear Materials*. Vol. 381. pp. 231–241. 2008.

Rosenberg, N.D., G.E. Gdowski, and K.G. Knauss. "Evaporative Chemical Evolution of Natural Waters at Yucca Mountain, Nevada." *Applied Geochemistry*. Vol. 16. pp. 1,231–1,240. 2001.

Rosenberg, N.D., K.G. Knauss, and M.J. Dibley. "Evaporation of J-13 Water: Laboratory Experiments and Geochemical Modeling." UCRL-ID-134852. Livermore, California: Lawrence Livermore National Laboratory. 1999.

SNL. "General Corrosion and Localized Corrosion of Waste Package Outer Barrier." ANL-EBS-MD-000003. Rev. 03. ACN 01, ERD 01. Las Vegas, Nevada: Sandia National Laboratories. 2007.

Spencer, R.J. "Sulfate Minerals in Evaporite Deposits." *Review in Mineralogy and Geochemistry*. Vol. 40. pp. 173–192. 2000.

Yang, L., R. Pabalan, P. Shukla, M. Juckett, X. He, K.T. Chiang, H. Gonzalez, and T. Ahn. "Corrosion of Alloy 22 Induced by Dust Deliquescence Brines." Rev. 3. San Antonio, Texas: Center for Nuclear Waste Regulatory Analyses. 2011.

Yang, I.C., Z.E. Peterman, and K.M. Scofield. "Chemical Analyses of Pore Water From Boreholes USW SD-6 and USW WT-24, Yucca Mountain, Nevada." *Journal of Contaminant Hydrology*. Vol. 1878. pp. 1–20. 2003.

Yang, I.C., P. Yu, G.W. Rattray, J.S. Ferarese, and J.N. Ryan. "Hydrochemical Investigations in Characterizing the Unsaturated Zone at Yucca Mountain, Nevada." Water-Resources Investigations Report 98-4132. Denver, Colorado: U.S. Geological Survey. 1998.

Yang, I.C., G.W. Rattray, and Y. Pei. "Interpretation of Chemical and Isotopic Data From Boreholes in the Unsaturated Zone at Yucca Mountain, Nevada." Water-Resources Investigations Report 96-4058. Denver, Colorado: U.S. Geological Survey. 1996.